UNIVERSITY OF CALIFORNIA, MERCED

On Nonlinear and Linear Schrödinger Equations: Computations and Theory

A dissertation submitted in partial satisfaction of
the requirements for the degree
Doctor of Philosophy

in

Applied Mathematics

by

Jessica Renee Taylor

Committee in charge:

Professor Boaz Ilan, Chair
Professor Arnold Kim
Professor Kevin Mitchell

2019

The Dissertation of Jessica Renee Taylor is approved, and it is acceptable in quality and form for publication on microfilm and electronically:

Prof. Boaz Ilan (Chair)

Prof. Arnold D. Kim

Prof. Kevin A. Mitchell

University of California, Merced
2019

To my parents, Charles & Dephany Taylor.
This work is as much yours as it is mine.

Contents

Signature Page . . . iii
Dedication . . . iv
List of Figures . . . vii
Acknowledgements . . . ix
Curriculum Vitae . . . x
Abstract . . . x

I Dipolar Nonlinear Schrödinger Equation 1

1 Introduction 2
1.1 Defining NLS . . . 2
1.2 Nonlinear Dispersive Waves: A History . . . 2
1.2.1 Water Waves . . . 2
1.2.2 Nonlinear Optics . . . 3
1.2.3 Quantum Mechanics . . . 4

2 Derivation of the NLS Equation in Dipolar BEC 5
2.1 Solitary-Body . . . 5
2.2 Many-Body . . . 6
2.3 Dipolar Interactions: Nonlinear Schrödinger Equation with Mean Terms . . . 6

3 Candlesticks and Collapse 8
3.1 Background . . . 8
3.2 Candlesticks . . . 11
3.3 Conclusions . . . 14

II Parity-Time Symmetric Linear Equation 16

4 Introduction 17

5 Background 18
5.1 Parity-Time Symmetry . . . 19

6 Symmetries and Degeneracies of BD Functions **20**
6.1 Symmetries 20
6.2 Perturbation analysis 22
6.2.1 The sign of β and irreversibility 24
6.2.2 Generalizations of the perturbation analysis 25
6.3 Computations 25
6.4 Perturbations 27
6.5 Numerical validation 30
6.5.1 Asymptotics for the integral (6.33) 31
6.6 Summary and conclusions 32

Appendix **32**

A Hamiltonian of Dipolar NLS Equation **34**
A.1 Hamiltonian Calculation 34
A.2 Numerical Implementation 35

B Accelerated Imaginary-Time Evolution (A-ITEM): **37**
B.1 Detail of Method 37
B.1.1 Amplitude Normalization: 38
B.2 Numerical Implementation 39

C Split-Step Fourier Transform (SSFT): **40**
C.1 Detail of Method 40
C.1.1 Linear part: $i\psi_t = -\psi_{xx}$ 40
C.1.2 Nonlinear part: $i\psi_t = -\psi|\psi|^2$ 41
C.2 Numerical Implementation 41
References 42

List of Figures

3.1 Candlestick condensate in a prolate trap with anisotropy parameter $\kappa = 4$,trap depth $V_0 = 0.1$, and condensate peak density $n_{\max} = 1$. (a) Density plot in the $r_\perp - z$ plane. (b) Iso-surface plot of the condensate (internal, teal) surrounded by the trap (magenta). 12

3.2 Collapse of a candlestick condensate. Plots of $|\psi(r_\perp, z, t)|^2$ at different times. Note the greater range in the vertical axis in the last plot. 12

3.3 Iso-surfaces corresponding to Fig. .3.2. 13

3.4 The peak density of the collapsing nucleus using a normal plot (a) and a log-log plot (b) with a best power-law fit [Eq. (3.12), dashed line]. 14

3.5 The nucleus' (a) radial width (dashes) and thickness (solid) as functions of time. (b) The nucleus' aspect ratio *vs.* its peak intensity during the collapse. 14

3.6 Normalized number of atoms of candlestick condensates as the chemical potential is varied. 15

5.1 Prior to first threshold: the associated linear spectrum real-valued. We observe that there exists a band gap. 19

6.1 The real parts of the first few band-dispersion functions corresponding to the potential (6.31) as a function of W_0. 26

6.2 The first two band dispersion functions of Eq. (5.3) with the potential (6.31) and (a1 & a2) $W_0 = 0.3$ (b1 & b2) $W_0 = W_{cr} = 0.5$. The real and imaginary parts are shown on the left and right panels, respectively. Here, the imaginary parts are identically zero. 27

6.3 Same as Fig. 6.2 with (a1 & a2) $W_0 = 1$; (b1 & b2) $W_0 = 2.65$. The imaginary parts form a complex conjugate pair of continuous and even functions. 28

6.4 Same as Fig. 6.3 with (a1 & a2) $W_0 = 2.98$; (b1 & b2) $W_0 = 3.1$. 29

6.5 The imaginary parts of the first two band-dispersion functions continued periodically to the adjacent Brillouin zones corresponding to the potential (6.31) with (a) $W_0 = 2.6$; (b) $W_0 = 2.98$; and (c) $W_0 = 3.1$. Here the imaginary parts are chosen as even, They are are continuous in $\mathcal{B}^*$ and can be ordered in non-decreasing values. 29

6.6 Same as Fig. 6.51, but with the imaginary parts chosen as odd functions. In this case, they are discontinuous at the edges of Brillouin zone, *i.e.*, at $k = \pm 1, \pm 3, \ldots$. 30

6.7 (a) The ratio β [Eq. (6.24)] computed using the perturbation analysis (6.24) and using the numerical approximation (6.38) for the potential (6.37) as a functions of the odd exponent P. (b) Same problem as (a) showing the log-log plot of $|\beta|$ obtained using the large-P asymptotics (6.36) compared with the numerical approximation (6.38). 32

Acknowledgments

I could not have completed this dissertation without the support of my advisor, Prof. Boaz Ilan. His encouragement, guidance and support has been present throughout my learning experience here at UC Merced in more ways than imagined. I would also like to thank my dissertation committee members, Prof. Arnold Kim and Prof. Kevin Mitchell for their perceptive feedback.

Lastly but certainly not least, I would like to thank my parents, Charles and Dephany Taylor. If it were not for their love and support throughout this entire journey, I have no idea where I would be today. One thing they have always told me was to "choose something I like and be good at it." Thank you, Mom and Dad. I hope I've made you proud.

Curriculum Vitae

Education

PhD	University of California, Merced Applied Mathematics Advisor: Prof. Boaz Ilan	2015 - present
MSc	University of California, Merced Applied Mathematics Advisor: Prof. Boaz Ilan	2015 - 2017
BSc	University of California, Merced Applied Mathematics, Physics Emphasis Advisors: Prof. Dimitrios Mitsotakis & Prof. Boaz Ilan	2011-2015

Abstract

This dissertation is composed of work on two types of Schrödinger equations: the nonlinear Schrödinger equation with dipolar interactions (dipolar NLS) and the parity-time ($\mathcal{PT}$) symmetric linear Schrödinger equation.

In the dipolar NLS work, we use a gradient-decent method to compute 3D ground states of the equation. We discover that highly-prolate traps, whose long axis is parallel to the dipoles, can give rise to "candlestick" ground states. Direct numerical simulations of the dipolar NLS equation reveal that the nucleus of the candlestick mode undergoes collapse, while obtaining a highly flat, pancake shape. The rate of this anisotropic collapse scales differently from what occurs in isotropic collapse. Stability analysis reveals a surprising cusp point in the mass vs. chemical potential curve, which may serve as a signature for these dynamics.

In addition, $\mathcal{PT}$ linear Schrödinger equations with complex $\mathcal{PT}$-symmetric periodic potentials are studied analytically and computationally. The possible symmetries of the band-dispersion functions and associated Floquet-Bloch states are identified. Using singular perturbation analysis, we show that band-dispersion functions become complex-valued following the closure of a spectral gap at a degenerate point. Furthermore, we analyze the effect of highly-localized perturbations using asymptotic techniques. The analytical results are elucidated by detailed computations. These results shed new light on the irreversible nature of the phase transition that takes place as the band-dispersion functions become complex.

Part I

Dipolar Nonlinear Schrödinger Equation

Chapter 1

Introduction

1.1 Defining Nonlinear Schrödinger Equations

Nonlinear Schrödinger (NLS) equations are universal equations in nonlinear dispersive wave theory. The NLS equation models a wide variety of phenomena in water waves, quantum mechanics and nonlinear optics. In water waves, the small-amplitude, deep water gravity waves suggest rogue (or "freak") waves. In quantum mechanics, the mean-field wavefunction of the NLS equation represents the evolution and dynamics of a Bose-Einstein condensate. In nonlinear optics, the classical field describes light propagating in planar waveguides and optical fibers. The commonality is that all aforementioned phenomena are quasi-monochromatic, slowly-varying waves propagating in weakly nonlinear dispersive media in the absence of dissipation.

In this work, we study a model which commonly arises in physics: the NLS equation with a cubic nonlinearity,

$$i\psi_t = -\Delta\psi + V(\mathbf{x})\psi + g|\psi|^2\psi \tag{1.1}$$

where $\psi = \psi(\mathbf{x}, t)$, Δ is the Laplacian and $V(\mathbf{x})$ is the potential. We will explore two types of NLS equations: a parity-time symmetric NLS equation and the NLS equation with dipolar interactions. Most of this work is on supercritical cases, such that $\sigma d = 3$, where σ scales the power of the nonlinearity and d is the dimension of the system. However, there is some work on the critical case $\sigma d = 2$.

1.2 Nonlinear Dispersive Waves: A History

1.2.1 Water Waves

Historically, the discipline of nonlinear dispersive waves has been ever growing. With the work of Stokes, nonlinear dispersive waves first started as a theory for water waves. In 1847, Stokes demonstrated the periodic wavetrain's

existence. In addition, he showed that the dispersion relation produces great changes in the qualitative behavior of nonlinear waves. Moreover, he made known many novel discoveries in nonlinear dispersive waves by not only extending linear works, but discovering new approaches to modeling phenomena. Stokes' deep analyses on water waves is considered to be the starting point for nonlinear dispersive waves.

In 1834, Russell observed an anomaly that he later named the "wave of translation." While on horseback, Russell viewed a boat in motion and noticed that when the boat suddenly stopped, the wave of water around the tip of the boat did not cease to exist; the wave continued forth with constant velocity. Russell titled this solitary wave as the wave of translation. Lord Rayleigh and Boussinesq later confirmed in 1864 the existence of a nonvanishing stationary wave in an irrotational and incompressible flow in shallow water, thus confirming Russell's observations.

Subsequently, in 1895, Korteweg and de Vries derived, arguably, the most significant move in solitary wave theory – the KdV equation. Korteweg and de Vries hoped to construct a model representing the behavior of a solitary wave in shallow fluid. By extending Lord Rayleigh's series expansions with their assumptions and adjoining a second-order derivative term representing surface tension effects, the KdV equation became a nonlinear evolution equation describing elongated, one dimensional, small amplitude waves, moving in a shallow fluid.

As time went by, significant advances in the water waves community slowed down. However, in 1965, Kruskal and Zabusky realized solitary waves and their interactions via computational analysis. By studying the Fermi-Pasta-Ulam-Tsingou equation, Kruskal and Zabusky formally named the solitary wave a *soliton*. Later, while studying the KdV equation, Kruskal and Zabusky discovered the inelasticity of solitons: the extraordinary characteristic that as solitons pass through each other, they remain the same, leaving each other with only a phase change.

Moreover on the nonlinear dispersive wavefront, in 1968, Zakarov derived the Nonlinear Schrödinger (NLS) equation for small amplitude, deep water waves. In this derivation, Zakharov accounted for water waves of infinite water depth. It was not until 1969, when Benney and Roskes derived the NLS equation for deep water waves of finite depth. The NLS water waves model presents rogue waves. Rogue waves are solitons that occur in open water caused by natural forces which bring into being spontaneous large waves.

1.2.2 Nonlinear Optics

In 1960, the laser was invented. With this development came a new field of study, nonlinear optics. It is called nonlinear optics because the atoms' response to high electromagnetic forces is no longer linear with respect to the electric field. The 1960s gave rise to rapid innovations in theory that led to better understanding of experiments. For instance, available optical fibers showed significant losses. Shortly after, the Stolen group used silica fibers, which had

fewer loses, to demonstrate nonlinear effects [67]. In 1964, Chiao, Gamire, and Townes derived the NLS equation for laser propagation in Kerr media and showed the significance of the ground state, also known as the Townes' mode [21]. However, in 1965, Kelley showed the collapse of the Townes' mode [39].

1.2.3 Quantum Mechanics

In 1924, Bose sent an article to Einstein regarding the statistics of photons. In this article, Bose derived Planck's quantum radiation principal without using classical physics. Einstein later protracted the ideas that Bose proposed therefore constructing the concept of a Bose gas, which is modeled by Bose-Einstein statistics. Einstein explained that cooling a bosonic gas to an extremely low temperature would condense them into the energetic ground state, resulting in a Bose-Einstein condensate (BEC).

As time passed, the development in BEC slowed down. However, in 1938, London speculated that BEC was the underlying quantum mechanical phenomenon of Superfluid ^{4}He. Through the 1930s – 1950s, the connection between BEC and superfluidity was studied in great detail. In 1950, quantitative evidence of London's proposition was realized. It was shortly after this realization that, in 1960, Gross and Pitaevskii derived the governing nonlinear evolution equation for Superfluid ^{4}He. This equation, the NLS equation, was set to model the underlying phenomena of Superfluid ^{4}He, thereby modeling BEC.

Bose-Einstein Condensation

Bose and Einstein predicted the phenomenon of Bose–Einstein condensation, which refers to bosonic systems that obey Bose-Einstein statistics. In quantum mechanics, bosons are particles that are represented by a wavefunction. A boson is symmetric with respect to this wavefunction. Due to this symmetry, bosons are not subject to the Pauli Exclusion Principle, which implies that two or more bosons can occupy a single quantum level simultaneously.

Consider a gas of bosons. When this gas is cooled within the range of absolute zero, we observe a collapse of the majority of bosons into ground state and the formation of a Bose-Einstein condensate (BEC). A BEC is a state of ultra-cold matter formed from a dilute bosonic gas.

The BEC exhibits particle-wave behavior and is therefore represented by a governing mean-field wavefunction. We assume that the state of the BEC is governed by the wavefunction. Therefore, this wavefunction represents the evolution and dynamics of the BEC. By studying the Nonlinear Schrödinger (NLS) equation with a linear potential in the semiclassical (or weakly-dispersive) regime, we find the wavefunction of a BEC. It is important to note, this NLS equation is commonly called the Gross-Pitaevskii equation. We present a derivation of the NLS equation from the Hamiltonian of the system.

Chapter 2

Derivation of the NLS Equation in Dipolar BEC

2.1 From the Hamiltonian to the Linear Schrödinger Equation: the Solitary-Body Problem

The Hamiltonian is a fundamental quantum mechanical operator that represents the total energy of the system. To develop the Hamiltonian, let us consider a solitary body in an infinite potential well. Here, the wavefunction of the body with a fixed total energy $\hat{H}$ can be written as

$$\psi(x,t) = u(x)e^{i(kx-\omega t)} \tag{2.1}$$

which is a standing wave with a spacially-dependent amplitude $u(x)$, wavelength k and frequency ω.

Using the quantum mechanical formulation, we have the following relationships: for the momentum $p = \hbar k$, and the energy $\hat{H} = \hbar\omega$. Therefore, in the Schrödinger system, the kinetic energy $\hat{T}$ is given by

$$\hat{T} = -\frac{\hbar^2}{2m}\nabla^2. \tag{2.2}$$

where m is the mass of the particle. The energy $\hat{V}$ due to the trapping potential is given by

$$\hat{V} = V(\mathbf{r}). \tag{2.3}$$

Therefore, the Schrödinger Hamiltonian is given by

$$\hat{H} = -\frac{\hbar^2}{2m}\nabla^2 + V(\mathbf{r}). \tag{2.4}$$

Substition of the definition of $\hat{H}$ into our Hamiltonian with respect to ψ yields the canonical Linear Schrödinger equation

$$i\hbar\frac{\partial}{\partial t}\psi = -\frac{\hbar^2}{2m}\nabla^2\psi + V(\mathbf{r})\psi. \tag{2.5}$$

2.2 Nonlinear Schrödinger Equation: the Many-Body Problem

The Nonlinear Schrödinger equation describes the evolution and dynamics of a Bose-Einstein condensate. To investigate the energy of the many-body bosonic system, we must use the formalism of the second quantization. Consider a dilute gas of N interacting bosons of mass m trapped in an external potential $V_{\text{ext}}(\mathbf{r})$. The Nonlinear Schrödinger Hamiltonian in the formalism of the second quantization is given by

$$\begin{aligned}\hat{\mathcal{H}} = &\int \hat{\Psi}^\dagger(\mathbf{r},t)\left[-\frac{\hbar^2}{2m}\nabla^2 + V_{\text{ext}}(\mathbf{r})\right]\hat{\Psi}(\mathbf{r},t) \\ &+ \int \hat{\Psi}^\dagger(\mathbf{r},t)\hat{\Psi}^\dagger(\mathbf{r}',t)V(\mathbf{r}-\mathbf{r}')\hat{\Psi}(\mathbf{r}',t)\hat{\Psi}(\mathbf{r},t)d\mathbf{r}'d\mathbf{r} \end{aligned} \tag{2.6}$$

where $\hat{\Psi}^\dagger$ and $\hat{\Psi}$ are field operators that correspond to the creation and annihilation of bosons and $V(\mathbf{r}-\mathbf{r}')$ is the short-range atom-atom interactions between particles.

$$\begin{aligned} i\hbar\frac{\partial}{\partial t}\hat{\Psi}(\mathbf{r},t) = &\left[-\frac{\hbar^2}{2m}\nabla^2 + V_{\text{ext}}(\mathbf{r})\right]\hat{\Psi}(\mathbf{r},t) \\ &+ \int \hat{\Psi}^\dagger(\mathbf{r},t)\hat{\Psi}^\dagger(\mathbf{r}',t)V(\mathbf{r}-\mathbf{r}')\hat{\Psi}(\mathbf{r}',t)\hat{\Psi}(\mathbf{r},t)d\mathbf{r}' \end{aligned} \tag{2.7}$$

Using the mean-field approximation, we decompose the field operator $\hat{\Psi}$ into a classical field and a perturbation, such that

$$\hat{\Psi}(\mathbf{r},t) = \psi(\mathbf{r},t) + \Psi'(\mathbf{r},t). \tag{2.8}$$

The classical field describes the condensed bosons and the perturbation, the non-condensed bosons. Next, substitute the expansion (2.8) into the Heisenburg-representation of the NLS equation (2.7) and collect the leading order terms. Finally, replace $V(\mathbf{r}-\mathbf{r}')$ with the effective potential $g\delta(\mathbf{r}-\mathbf{r}')$ because for a dilute and cold gas, only low energy, two-body collisions are relevant [33]. The collisions are described by a single parameter, the s-wave scattering length. These substitutions return the well-known NLS equation

$$i\hbar\frac{\partial}{\partial t}\psi(\mathbf{r},t) = \left[-\frac{\hbar^2}{2m}\nabla^2 + V_{\text{ext}}(\mathbf{r}) + g|\psi(\mathbf{r},t)|^2\right]\psi(\mathbf{r},t). \tag{2.9}$$

2.3 Dipolar Interactions: Nonlinear Schrödinger Equation with Mean Terms

In 1995, the first BEC was experimentally realized by Cornell and Wieman [7] In the wake of this discovery, BECs are now considered to be the underlying

quantum mechanical structures for a wide variety of phenomena, ranging fields such as optics to superfluidity. Due to this versatility, there exists a wide interest in the control and stabilization of BECs. A known and practiced way of stabilizing a BEC is to induce dipolar interactions.

A 3D dipolar BEC is described by the (3+1)-dimensional NLS equation with dipolar interactions given below:

$$\begin{aligned} i\hbar\frac{\partial}{\partial t}\psi(\mathbf{r},t) = &-\frac{\hbar^2}{2m}\nabla^2\psi(\mathbf{r},t) + V_{\text{ext}}(\mathbf{r})\psi(\mathbf{r},t) \\ &+ |\psi|^2\psi + \int U_{\text{dip}}(\mathbf{r}-\mathbf{r}')|\psi(\mathbf{r}')|^2 d\mathbf{r}\psi(\mathbf{r},t) \end{aligned} \tag{2.10}$$

with the Thomas-Fermi long-range dipolar interaction potential is given by

$$U_{\text{dip}}(\mathbf{r}-\mathbf{r}') = g\left(\frac{1}{|\mathbf{r}-\mathbf{r}'|^3} - \frac{3(z-z')}{|\mathbf{r}-\mathbf{r}'|^5}\right) \tag{2.11}$$

where the dipoles lie at points $\mathbf{r}$ and $\mathbf{r}'$ aligned by an external field.

As written in the NLS equation, let

$$V_{\text{dip}}(\mathbf{r}) = \int U_{\text{dip}}(\mathbf{r}-\mathbf{r}')d\mathbf{r} \tag{2.12}$$

be the energy induced by the dipolar interactions.

The energy contribution (2.12) can be simplified by making use of the relationship

$$\frac{1}{|\mathbf{r}-\mathbf{r}'|^3} - \frac{3(z-z')}{|\mathbf{r}-\mathbf{r}'|^5} = -\frac{\partial^2}{\partial z^2}\left(\frac{1}{|\mathbf{r}-\mathbf{r}'|}\right) - \frac{4\pi}{3}\delta(\mathbf{r}-\mathbf{r}'). \tag{2.13}$$

This allows our dipolar potential to become

$$V_{\text{dip}}(\mathbf{r}) = -\tilde{g}\left(\frac{\partial^2\phi(\mathbf{r})}{\partial z^2} + \frac{1}{3}|\psi|^2\right) \tag{2.14}$$

where

$$\phi(\mathbf{r}) = \int \frac{|\psi|^2}{|\mathbf{r}-\mathbf{r}'|}d\mathbf{r}. \tag{2.15}$$

Here, ϕ satisfies $\Delta\phi = |\psi|^2$ and represents the "electrostatic potential due to the charge distribution $|\psi|^2$" [58]. Therefore, we are left with an NLS equation with mean terms:

$$i\hbar\frac{\partial}{\partial t}\psi(\mathbf{r},t) = -\frac{\hbar^2}{2m}\nabla^2\psi(\mathbf{r},t) + V_{\text{ext}}(\mathbf{r})\psi(\mathbf{r},t) + g_d\left(|\psi|^2 + \varphi_{zz}\right)\psi. \tag{2.16}$$

Chapter 3

Candlestick Modes and Anisotropic Collapse of Dipolar Bose-Einstein Condensates

3.1 Background

Wave collapse is one of the hallmarks of nonlinear dispersive waves in a wide range of systems, including plasma physics [61], hydrodynamics [77], optics [53], and Bose-Einstein condensates (BECs) [28, 45, 74, 32]. Collapse occurs when an attracting (focusing) nonlinearity overcomes dispersion. This intrinsic feature of nonlinear waves has been investigated for more than 50 years, leading to many theoretical advances in the framework of the nonlinear Schrödinger equation [68, 34]. In general, it is found that collapse occurs with a self-similar profile [31]. When the nonlinear interactions are local and isotropic, as is the case for the optical Kerr effect in bulk media and in some BECs, the wave collapses isotropically to a point. Radially-symmetric ring collapse in the isotropic NLS equation has also been studied and observed in optics [35, 73, 36, 10]. BECs of ^{52}Cr and other atoms give rise to strong dipole-dipole interactions [58]. Dipolar effects are also inherently anisotropic, leading to anisotropic solitons [71] and anisotropic superfluidity [70].

Since BECs are prepared in energetic ground states, the characterization of these ground states is central to their dynamics. However, the theory of dipolar BEC ground states in three spatial dimensions (3D) is not well developed. Almost all the previous analytical and computational studies of dipolar BECs have relied on lower-dimensional approximations. In this work, we use an accurate numerical method to compute directly the 3D ground states of dipolar BECs trapped in anisotropic harmonic potentials. We find that in a highly-prolate trap, the ground state has an elongated candlestick-like structure, with a larger nucleus flanked by two smaller nodes. Using direct simulations of the dipolar Gross-Pitaevskii equation, we show that the central node flattens and shrinks, eventually undergoing anisotropic collapse. We show that the collapsing nucleus deforms from an initially spherical shape to a pancake shape, which is retained during the collapse dynamics. The rate of this anisotropic collapse is found to scale differently from the corresponding isotropic case. We also find

the mass *vs.* chemical potential curve, which reveals a cusp point that has not been reported in other nonlinear systems. We raise the conjecture that such a cusp point is associated with anistropic collapse dynamics.

We begin by recapitulating some of the key properties of dipolar BECs (see [40, 58, 8, 44].). The dynamics of a dipolar BEC can be described using the dipolar Gross-Pitaevskii equation for the mean-field $\psi(\boldsymbol{r}, t)$,

$$i\hbar\psi_t(\boldsymbol{r}, t) = \Big[-\frac{\hbar}{2m}\nabla^2 + V_{\text{ext}}(\boldsymbol{r}) + g_1|\psi(\boldsymbol{r}, t)|^2 \tag{3.1}$$

$$+ g_2 \int_{\mathbb{R}^3} V_{\text{dip}}\left(|\psi|^2\right)(\boldsymbol{r} - \boldsymbol{r}')|\psi(\boldsymbol{r}', t)|^2 d\boldsymbol{r}'\Big]\psi(\boldsymbol{r}, t), \tag{3.2}$$

where $\boldsymbol{r} = (x, y, z)$, $\nabla^2 = \partial_x^2 + \partial_y^2 + \partial_z^2$ is the 3D Laplacian, $V_{\text{ext}}(\boldsymbol{r})$ is an external potential, and the terms with g_1 and g_2 correspond to the local (short-range) and dipolar (long-range) interactions, respectively. The dipolar potential is

$$V_{\text{dip}}\left(|\psi|^2\right)(\boldsymbol{r}) = \frac{1 - 3\cos^2(\theta)}{|\boldsymbol{r}|^3} \tag{3.3}$$

where θ is the angle between $\boldsymbol{r}$ and the dipole axis, which we assume is aligned along the z-axis. We are interested a regime where the short-range interactions are repulsive, *i.e.*, $g_1 > 0$, and the long-range interactions are such that $g_2 < 0$. Due to the variation of the sign of (3.3), the dipolar interactions are give rise to both attractive and repulsive effects. Therefore, in the regime we consider, the dipolar interactions are the sole quasi-attractive mechanism.

Two important conserved quantities of Eq. (3.1) are the total number of atoms (analogous to the total power in optics),

$$N[\psi] = \int |\psi|^2 d\boldsymbol{r}\ , \tag{3.4}$$

and the total energy (Hamiltonian) of the condensate,

$$E[\psi] = \frac{1}{2}\int_{\mathbb{R}^3} \big[\hbar^2|\nabla\psi|^2 + 2V|\psi|^2 + g_1|\psi|^4 \tag{3.5}$$

$$+ g_2 \int_{\mathbb{R}^3} V_{\text{dip}}\left(|\psi|^2\right)(\boldsymbol{r} - \boldsymbol{r}')|\psi(\boldsymbol{r}', t)|^2 d\boldsymbol{r}'|\psi|^2\Big] d\boldsymbol{r}.$$

BECs are formed in the energetic ground state, which can be characterized as follows. Assuming a time-harmonic solution, $\psi(\boldsymbol{r}, t) = u(\boldsymbol{r})\exp(-i\mu t)$, where μ is called the chemical potential, leads to the stationary dipolar GP equation for the mode structure function $u(\boldsymbol{r})$,

$$\mu\hbar u(\boldsymbol{r}) = \Big[-\frac{\hbar^2}{2m}\nabla^2 + V_{\text{ext}}(\boldsymbol{r}) + g_1|u(\boldsymbol{r})|^2 \tag{3.6}$$

$$+ g_2 \int_{\mathbb{R}^3} V_{\text{dip}}\left(|u|^2\right)(\boldsymbol{r} - \boldsymbol{r}')|u(\boldsymbol{r}')|^2 d\boldsymbol{r}'\Big] u(\boldsymbol{r}).$$

Equation (3.6) admits infinitely many solutions. The ground state is the non-trivial minimizer of the total energy. It can be shown that the ground state is unique and non-negative [46]. It is instructive and useful to reformulate Eq. (3.1) as (see [30, 58])

$$i\hbar\psi_t(\boldsymbol{r},t) = \left[-\frac{\hbar}{2m}\nabla^2 + V_{\text{ext}}(\boldsymbol{r}) + (g_1-g_2)|\psi(\boldsymbol{r},t)|^2 + 3g_2\varphi_{zz}(\boldsymbol{r})\right]\psi \ ,$$

$$\nabla^2\varphi(\boldsymbol{r},t) = |\psi(\boldsymbol{r},t)|^2 \ , \tag{3.7a}$$

where $\varphi(\boldsymbol{r},t)$ is an auxiliary nonlinear potential that decays to zero as $|\boldsymbol{r}| \to \infty$. One advantage of this formulation is that it circumvents the highly-singular integral in (3.3). It is remarkable that system (3.7) has the same mathematical structure [1] as the Benney-Roskes / Davey-Stewartson system, which describes surface waves in a fluid of finite depth [15, 27] and intense light propagation coupled to an electrostatic field [4, 5, 26]. This system has been studied extensively in (2+1)-dimensions. In particular, in [3] it was shown that the collapsing solution becomes (mildly) anisotropic. However, almost all the previous studies have been in (2+1)-dimensions and not much is known about the solutions of this system in three spatial dimensions.

Previous studies of dipolar BECs ground states have used variational methods to characterize the ground states, cf. [76, 47, 56, 30, 57, 16, 48, 2]. In the variational approach, one assumes a Gaussian or other profile for the shape of the mode and derives the relationships between its amplitude and width. However, as we show below, in certain parameter regimes the structure of the ground state cannot be well-approximated with a Gaussian or any other simple analytic profile. Here, we use a numerical approach to compute the ground states.

To fix some of the parameter regime, we set $\hbar = m = 1$ and the short and long-range interaction coefficients as $g_1 = 1$ and $g_2 = -1$. This is equivalent to normalizing the physical variables to the characteristic nonlinear length scale of the system, which is determined by the atomic scattering length. We use an anisotropic harmonic external trapping potential,

$$V_{\text{ext}}(\boldsymbol{r}) = V_0\left[x^2 + y^2 + (\kappa z)^2\right] \ , \tag{3.8}$$

where V_0 is the potential depth and κ is the anisotropy parameter, *i.e*, $\kappa < 1$ and $\kappa > 1$ correspond to a prolate (cigar-shaped) and oblate (pancake-shaped) potentials, respectively. Since the trap is radially symmetric in the $x-y$ plane, the condensate inherits this symmetry. Thus, we denote the planar radial coordinate (not to the confused with $|\boldsymbol{r}| = \sqrt{x^2+y^2+z^2}$) as

$$r_\perp = \sqrt{x^2+y^2}$$

and proceed to solve the stationary and time-dependent problems in the $(r_\perp, z)$ and $(r_\perp, z, t)$ coordinate systems, respectively. To solve the stationary equation (3.6) we employ the Accelerated Imaginary-Time Evolution Method (A-ITEM), which is a gradient-decent method for computing ground states of nonlinear dispersive equations [75]. In particular, we iterate the A-ITEM scheme

for Eq. (3.7) [recast in terms of $u(\boldsymbol{r})$] while normalizing the peak density of the condensate,

$$n_{\max} = \max_{\boldsymbol{r}} |u(\boldsymbol{r})|^2, \tag{3.9}$$

to a constant of choice. The chemical potential is recovered in each iteration from the relationship

$$\mu = E[\psi] + \frac{1}{2}\left[\int_{\mathbb{R}^3} g_1|u|^4 + g_2 \int_{\mathbb{R}^3} V_{\rm dip}\left(|u|^2\right)(\boldsymbol{r}-\boldsymbol{r}')|u(\boldsymbol{r}',t)|^2 d\boldsymbol{r}'|u|^2\right]. \tag{3.10}$$

There is a one-to-one relation between $n_{\max}$ and μ. Therefore, the ground state can be defined by either of them. Convergence is obtained when the relative differences between successive iterations of μ is smaller than 10^{-5}. In all cases, this requires at most a few thousand iterations.

3.2 Candlestick Modes

We find that prolate traps can produce a "candlestick"-shaped condensate, whose nucleus is flanked by two smaller nodes (see Fig. 3.1). In this figure we represent the condensate in two different ways. First, as the density plot of $|\psi(\boldsymbol{r})|^2 = u^2(\boldsymbol{r})$ in the $r_\perp - z$ plane. Since the condensate is radially symmetric in the $x-y$ plane, the 3D ground state solution is computed by rotation of $u(r_\perp, z)$ around the z-axis. Fig. 3.1(b) presents an iso-surface plot of this 3D function, "sliced" at the contour level of 0.4, or 40% of the peak density. The candlestick modes arise when the trap is highly anisotropic and shallow. We emphasize that this occurs in spite of the trap having a single well, because of the anisotropic nature of the long-range interactions.

To investigate the evolution of the ground states, we solve Eq. (3.7). Figures 3.2 and 3.3 present four snapshots of the density and iso-surface dynamics of the solution. The initial excitation for this computation was the condensate in Fig. 3.1 with a 2% amplitude perturbation, *i.e.*, $\psi(0,t) = 1.02\,u(\boldsymbol{r})$. We note that the collapse pattern in Fig. 3.1(b) resembles qualitatively the collapse patterns observed experimentally by Metz *et al.* [52] in ^{52}Cr BECs. The nucleus might appear to break off from the two nodes. However, the nodes remain in tact and close to the nucleus. We point out that the two nodes do not appear in the last iso-surface plot, because their peak densities are much smaller than the peak density of the nucleus.

To study the collapse process of the candlestick condensate, we denote its peak density as

$$n_{\max}(t) = \max_{\boldsymbol{r}} |\psi(\boldsymbol{r},t)|^2 \ . \tag{3.11}$$

Figure 3.4(a) shows $n_{\max}(t)$ for the collapse in Fig. 3.2, which blows-up at $T_c \approx 59$. Here $n_{\max}(0) = 1$, so $n_{\max}(t)$ is also the relative change of the peak

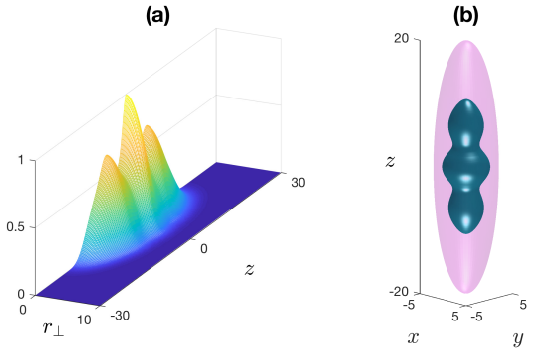

Figure 3.1: Candlestick condensate in a prolate trap with anisotropy parameter $\kappa = 4$,trap depth $V_0 = 0.1$, and condensate peak density $n_{\max} = 1$. (a) Density plot in the $r_\perp - z$ plane. (b) Iso-surface plot of the condensate (internal, teal) surrounded by the trap (magenta).

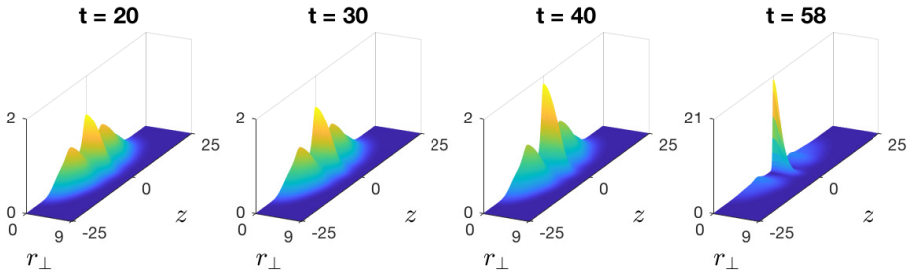

Figure 3.2: Collapse of a candlestick condensate. Plots of $|\psi(r_\perp, z, t)|^2$ at different times. Note the greater range in the vertical axis in the last plot.

density. Figure 3.4(b) shows that, near the collapse time, the peak density scales as

$$n_{\max}(t) \sim (T_c - t)^{-3/4} \ . \tag{3.12}$$

Figure 3.5(a) shows the radial width and thickness of the nucleus, which are recovered from the full-width at half-max of $|\psi(r_\perp, z, t)|^2$ along the radial and z-axes, respectively. After an initial stage ($t \leq 15$), the thickness $L_z(t)$ decreases linearly with $T_c - t$. Therefore, the peak density scales with the

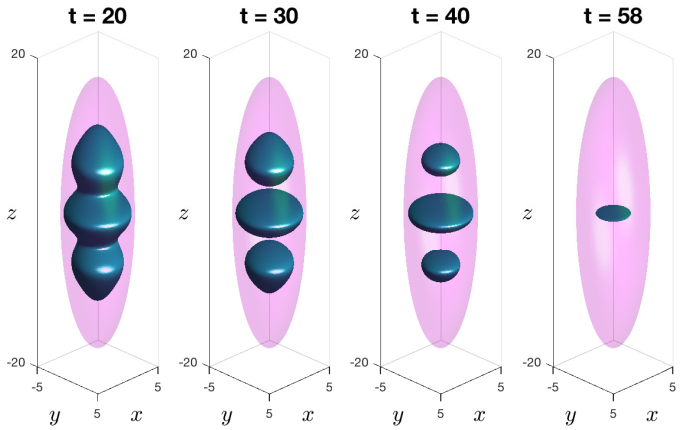

Figure 3.3: Iso-surfaces corresponding to Fig. .3.2.

thickness approximately as

$$n_{\max}(t) \sim [L_z(t)]^{-3/4}. \tag{3.13}$$

Figure 3.5(a) also shows that the nucleus, which is initially almost spherical, flattens more quickly than it shrinks in the radial directions, leading to a pancake-shaped collapse. This is further demonstrated in Fig. 3.5(b), which shows the aspect ratio of the nucleus plotted against its peak density during the collapse. The limiting aspect ratio near the collapse time is greater than 7, *i.e*, the pancake is quite flat, as also indicated by Figs. 3.2 and 3.3. In contrast, for the analogous system in (2+1)-dimensions, the collapsing solution is mildly anisotropic [3].

It is interesting to compare these results with the collapse in isotropic NLS equations. In NLS theory, the collapse (blowup) rate has has been studied extensively [68, 34]. Both the short-range and long-range nonlinearities in the dipolar GP equation (3.1) are cubic. For the 3D cubic NLS equation, it has long been conjectured and recently proven [51] that, as the solution approaches the collapse time, its width decreases as $L \sim \sqrt{T_c - t}$, and its peak density increases as $n_{\max} \sim (T_c - t)^{-1}$. Therefore, $n_{\max} \sim 1/L^2$. These exponents are quite different from (3.12) and (3.13), further demonstrating the unique nature of anisotropic collapse.

We also study the linear stability of these ground states. Figure 3.6 shows the (normalized) total number of atoms (3.4) in the ground state as functions of the chemical potential. The potential depth is $V_0 = 0.1$ and anisotropy parameter is $\kappa = 0.25$. This graph is obtained by computing the ground states with peak densities in the range $0.1 \leq n_{\max} \leq 36$ and using Eq. (3.10) to map $n_{\max}$ to μ. In NLS theory, it is known that the ground state is amplitude-stable when $dN/d\mu > 0$, where $N(\mu) = N[\psi(\cdot;\mu)]$ is the number of atoms (3.4) or total mass [72, 66, 37]. In this sense, Fig. 3.6 indicates that the ground states are linearly stable, despite their nonlinear instability. However, what is

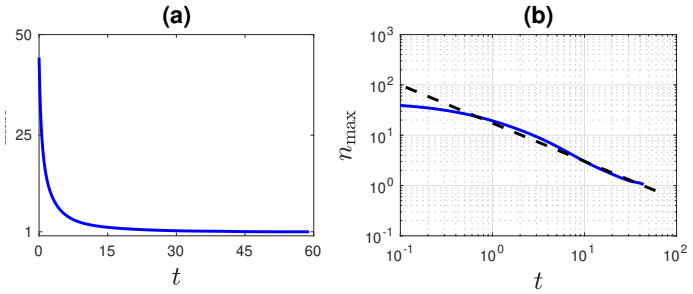

Figure 3.4: The peak density of the collapsing nucleus using a normal plot (a) and a log-log plot (b) with a best power-law fit [Eq. (3.12), dashed line].

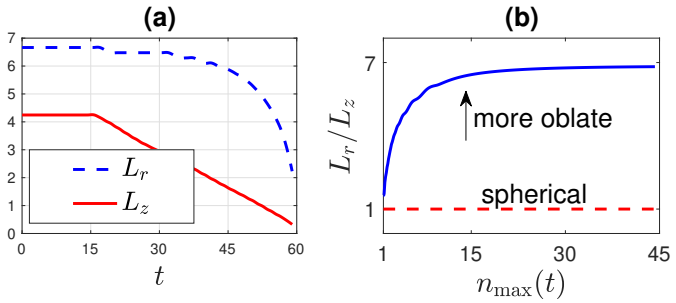

Figure 3.5: The nucleus' (a) radial width (dashes) and thickness (solid) as functions of time. (b) The nucleus' aspect ratio *vs.* its peak intensity during the collapse.

truly surprising about Fig. 3.6 is the cusp point, which occurs at $n_{\max} \approx 1$. To our knowledge, this is the first system in which a cusp point in $N(\mu)$ has been reported. Moreover, we note that, as $n_{\max}$ increases, *i.e*, as one traces the ground states along the $N(\mu)$ curve, the nucleus becomes much larger compared with the side nodes. This mimics what happens during the collapse dynamics. Based on this observations, we conjecture that the cusp point in the $N(\mu)$ curve could be a signature of the anisotropic collapse of these ground states.

3.3 Conclusions

In conclusion, our computational results show that long-range dipolar interactions in a BEC can give rise to highly anisotropic condensate ground states that undergo anisotropic collapse, which occurs at a different rate from the isotropic case. Here, we observe that the candlestick ground state undergoes a 2D surface collapse as opposed to the canonical 1D point collapse. This demonstrates that anisotropic long-range interactions can lead to localized nonlinear waves with unique collapse patterns and kinetic properties, which could open

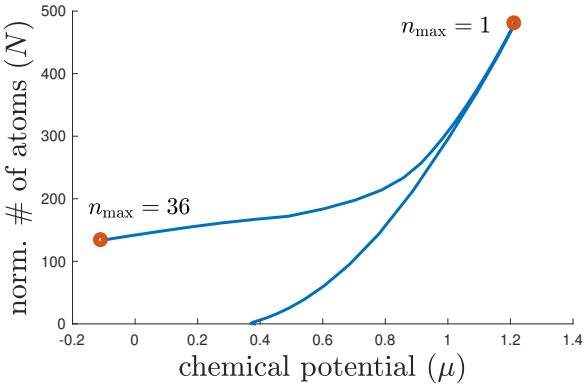

Figure 3.6: Normalized number of atoms of candlestick condensates as the chemical potential is varied.

up new venues for exploring many-body collective excitations.

Part II

Parity-Time Symmetric Linear Equation

Chapter 4

Introduction

In the past two decades, Schrödinger equations with complex $\mathcal{PT}$-symmetric potentials have garnered much attention in the math and physics literatures due to their remarkable properties. These equations evoke fundamental questions about quantum mechanics [12] and have potential application to several other areas of physics, such as superconductivity [62, 22], Bose-Einstein condensates [18], and optics (cf. [50, 14, 59, 20, 9]). Physically, the real part of the potential can be used to confine waves (or wave functions), while its imaginary part corresponds to dissipative or gain mechanisms.

When the potential is real and periodic (lattice potential), spectral theory, also known as Floquet-Bloch theory, is well developed (cf. [60, 29, 43]). Band-dispersion functions, which can be thought of as "extended eigenvalues", play a central role in this theory and form the basis for much of condensed-matter physics [41, 38]. However, Floquet-Bloch theory is much less developed for complex potentials, since these problems are non self-adjoint. One of the remarkable properties of complex $\mathcal{PT}$-symmetric potentials is that the resulting band-dispersion functions can be entirely real, in-spite of the non-self-adjointness of the equations (cf. [24, 25]). This raises several questions about the emergence of complex band-dispersion functions and their symmetries. In this study, we identify the symmetries of the band-dispersion functions and their associated Floquet-Bloch states. In particular, we show that the band-dispersion functions can be chosen as either symmetric or anti-symmetric. These symmetries are "inherited" from the $\mathcal{PT}$ symmetry of the potential. In addition, we show in a perturbative sense that the closure of a direct spectral gap directly follows the formation of degenerate point in the band-dispersion functions. The case of highly-localized potentials is examined using asymptotic techniques. The symmetries and the perturbation / asymptotic results are elucidated by computations.

Chapter 5

Background

As a background, we review some of the results of spectral theory for Schrödinger equation with real periodic potentials. Consider the Schrödinger equation,

$$(-\Delta + V)u(\boldsymbol{x}) = Eu(\boldsymbol{x}) \ , \tag{5.1}$$

where $\boldsymbol{x} \in \mathbb{R}^d$, $\Delta = \sum_{j=1}^{d} \partial_{x_j x_j}$ is the Laplacian, $V(\boldsymbol{x})$ is real and periodic (also called a lattice potential), $E \in \mathbb{C}$ is an eigenvalue (also called frequency, propagation constant, or chemical potential), and $u(\boldsymbol{x}; E) \in H^1(\mathbb{R}^d)$ its associated eigenfunction. Let $\mathcal{B}$ denote the fundamental period cell and $\mathcal{B}^*$ denote the first Brillouin zone of the dual basis (or dual lattice). A point $\boldsymbol{k} \in \mathcal{B}^*$ is called *quasi-momentum* and the eigenfunctions $u(\boldsymbol{x})$ are called *Floquet-Bloch states*.

For every $\boldsymbol{k} \in \mathcal{B}^*$, the Floquet-Bloch state can be written as

$$u(\boldsymbol{x}, \boldsymbol{k}) = p(\boldsymbol{x}, \boldsymbol{k}) e^{i\boldsymbol{k}\cdot\boldsymbol{x}} \ , \tag{5.2}$$

where $p(\boldsymbol{x}, \boldsymbol{k})$ is periodic in $\boldsymbol{x} \in \mathcal{B}$. Substituting this ansatz into (5.1) gives

$$\left[-(\nabla + i\mathbf{k})^2 + V(\boldsymbol{x}) \right] p(\boldsymbol{x}, \boldsymbol{k}) = E(\boldsymbol{k}) p(\boldsymbol{x}, \boldsymbol{k}) \ , \tag{5.3}$$

where $E(\boldsymbol{k})$ is called a *band-dispersion function*. Since $V(\boldsymbol{x})$ is real, the problem is self-adjoint and the band-dispersion functions are real. They form a sequence continuous functions that can be ordered in non-decreasing values tending to infinity as

$$E_1(\boldsymbol{k}) \leq E_2(\boldsymbol{k}) \leq E_3(\boldsymbol{k}) \leq \dots \ . \tag{5.4}$$

The operator on the left-hand side of (5.3) is invariant under the transformation $\boldsymbol{k} \to -\boldsymbol{k}$ and complex conjugation. Therefore, if $E(\boldsymbol{k})$ and $p(\boldsymbol{x}, \boldsymbol{k})$ are an eigenpair, so are $E^*(-\boldsymbol{k})$ and $p^*(\boldsymbol{x}, -\boldsymbol{k})$. This symmetry, together with the continuity of $E(\boldsymbol{k})$ and the ordering (5.4), imply that

$$E_j(-\boldsymbol{k}) = E_j(\boldsymbol{k}) \ , \quad \forall j \in \mathbb{N} \ . \tag{5.5}$$

When $\max_{\boldsymbol{k}} E_j(\boldsymbol{k}) < \min_{\boldsymbol{k}} E_{j+1}(\boldsymbol{k})$, there is a *spectral gap* between these two sequential functions. A *direct bandgap* occurs when there is an isolated $\boldsymbol{k}_\star$, such that

$$\boldsymbol{k}_\star = \arg\max E_j(\boldsymbol{k}) = \arg\min E_{j+1}(\boldsymbol{k}) \ ,$$

where these maxima and minima can be local or global. When a direct bandgap closes under a small perturbation, it does so at an isolated point, called *exceptional point*, such that

$$E_j(\boldsymbol{k}_\star) = E_{j+1}(\boldsymbol{k}_\star) \ .$$

Spectral gaps and their closure are essential in the physics of semiconductors and other materials.

5.1 Parity-Time Symmetry

Among many versions of linear Schrödinger equations, there exists a special class,

$$i\psi_t(\mathbf{x},t) = -\Delta\psi(\mathbf{x},t) + V(\mathbf{x})\psi(\mathbf{x},t), \tag{5.6}$$

where $\mathbf{x} \in \mathbb{R}^d$, $g \in \mathbb{R}$, $\sigma > 0$, $t \geq 0$, Δ is the Laplacian, and $V(\mathbf{x})$ is a linear potential. Eq. (5.6) is interesting because it exhibits parity-time ($\mathcal{PT}$) symmetry. $\mathcal{PT}$-symmetry is defined when a system remains invariant under spatial parity and time reversal, $\mathbf{x} \to -\mathbf{x}$, $t \to -t$, and $\psi \to \psi^*$.

A key component of quantum mechanics is the Hermiticity of an operator and thus the associated physical observable [54]. Due to Hermiticity, the spectra of these operators is always real. This fundamental notion was challenged when Bender and Boettcher discovered that classes of linear Schrödinger equations, corresponding to non-Hermitian Hamiltonians that exhibit $\mathcal{PT}$-symmetry, possess real and positive spectra 5.1. For linear Schrödinger equations with real-valued, $\mathcal{PT}$-symmetric potentials, the spectra remains real. Here, it is said that the $\mathcal{PT}$-symmetry of the system holds. [13].

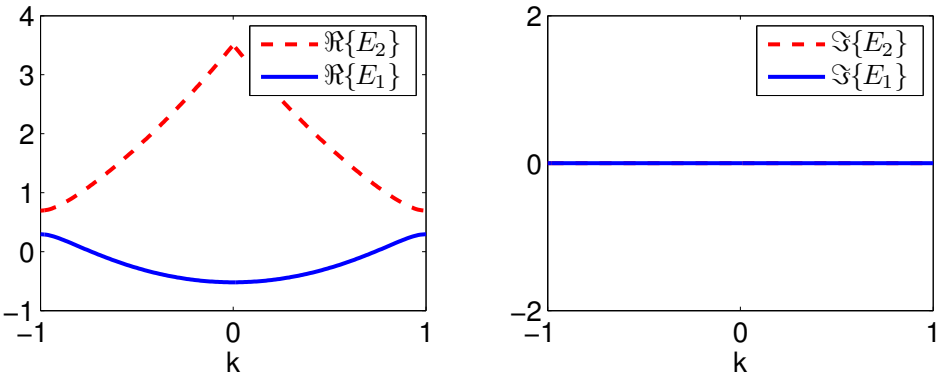

Figure 5.1: Prior to first threshold: the associated linear spectrum real-valued. We observe that there exists a band gap.

Chapter 6

Symmetries and degeneracies of band-dispersion functions of Schrödinger equations with complex $\mathcal{PT}$-symmetric periodic potentials

6.1 Symmetries of band-dispersion functions for $\mathcal{PT}$-symmetric potentials

In this section we identify the symmetries of band-dispersion functions for $\mathcal{PT}$-symmetric potentials. We assume that the potential function in (5.1) is complex $\mathcal{PT}$-symmetric and periodic, *i.e.*,

$$V^*(\boldsymbol{x}) = V(-\boldsymbol{x}), \quad V(\boldsymbol{x}+\boldsymbol{l}) = V(\boldsymbol{x}) \quad \forall \boldsymbol{x} \in \mathbb{R}^d \ , \tag{6.1}$$

where * stands for complex conjugation and $\boldsymbol{l}$ is the fundamental period. This implies that

$$V(\boldsymbol{x}) = V_R(\boldsymbol{x}) + V_I(\boldsymbol{x}) \ , \quad V_R(-\boldsymbol{x}) = V_R(\boldsymbol{x}), \quad V_I(-\boldsymbol{x}) = -V_I(\boldsymbol{x}) \ . \tag{6.2}$$

Here, the evenness property (5.5) does not hold. However, using (6.1) the operator on the left-hand side of (5.3) is invariant under $\boldsymbol{x} \to -\boldsymbol{x}$ and complex conjugation. Therefore, if $E(\boldsymbol{k})$ and $p(\boldsymbol{x},\boldsymbol{k})$ are an eigenpair, so are $E^*(\boldsymbol{k})$ and $p^*(-\boldsymbol{x},\boldsymbol{k})$. This implies that the band-dispersion functions and eigenfunctions can have the symmetries

$$E^*(\boldsymbol{k}) = E(\boldsymbol{k}), \quad p^*(-\boldsymbol{x},\boldsymbol{k}) = p(\boldsymbol{x},\boldsymbol{k}) \ . \tag{6.3}$$

Hence, for every $\boldsymbol{k} \in \mathcal{B}^*$, the band-dispersion functions are either real (they need not be distinct) or form a complex-conjugate pair. Their real parts may be chosen to be continuous and ordered in non-decreasing values,

$$\operatorname{Re} E_1(\boldsymbol{k}) \le \operatorname{Re} E_2(\boldsymbol{k}) \le \operatorname{Re} E_3(\boldsymbol{k}) \le \dots \ . \tag{6.4}$$

Several questions arise, including

1. Does $\mathcal{PT}$ symmetry imply any symmetry as $\boldsymbol{k} \to -\boldsymbol{k}$?

2. Is $\boldsymbol{k} \mapsto \operatorname{Im} E(\boldsymbol{k})$ continuous?

3. How should $\operatorname{Im} E(\boldsymbol{k})$ be ordered?

These questions are related to each other. To address them, let us assume that a band-dispersion function is not identically real across $\mathcal{B}^*$. Using (6.3) there are two linearly independent band-dispersion functions and associated eigenfunctions, which can be denoted and decomposed as

$$E_\pm(\boldsymbol{k}) = E_R(\boldsymbol{k}) \pm iE_I(\boldsymbol{k}) \ , \tag{6.5a}$$

$$p_\pm(\boldsymbol{x},\boldsymbol{k}) = p_R(\boldsymbol{x},\boldsymbol{k}) \pm ip_I(\boldsymbol{x},\boldsymbol{k}) \ . \tag{6.5b}$$

Substituting (6.5) into (5.3), using (6.2), and separating the real and imaginary parts leads to the coupled system

$$[L_R - E_R(\boldsymbol{k})]\, p_R(\boldsymbol{x},\boldsymbol{k}) = [L_I - E_I(\boldsymbol{k})]\, p_I(\boldsymbol{x},\boldsymbol{k}) \ , \tag{6.6a}$$

$$[L_R - E_R(\boldsymbol{k})]\, p_I(\boldsymbol{x},\boldsymbol{k}) = -[L_I - E_I(\boldsymbol{k})]\, p_R(\boldsymbol{x},\boldsymbol{k}) \ , \tag{6.6b}$$

where

$$L_R = -\Delta + V_R(\boldsymbol{x}) + \boldsymbol{k}^2 \ , \tag{6.7a}$$

$$L_I = -2\boldsymbol{k}\cdot\nabla + V_I(\boldsymbol{x}) \ . \tag{6.7b}$$

Inspecting symmetries of (6.6)–(6.7) as $\boldsymbol{k} \to -\boldsymbol{k}$, it is *possible* to choose

$$E_R(-\boldsymbol{k}) = E(\boldsymbol{k}) \ , \quad E_I(-\boldsymbol{k}) = -E_I(\boldsymbol{k}) \ , \tag{6.8}$$

with likewise symmetries for $\boldsymbol{k} \to p(\cdot,\boldsymbol{k})$. Hence, the band-dispersion functions may be *chosen* to have the $\mathcal{PT}$ symmetry

$$E^*(-\boldsymbol{k}) = -E(\boldsymbol{k}) \ . \tag{6.9}$$

We note that symmetries (6.3) and (6.9) neither contradict nor follow from each other. However, symmetry (6.9) implies that $\operatorname{Im} E(\boldsymbol{k})$ can be discontinuous. Indeed, an odd function that is also continuous must be zero at the origin, which is not the case in general. The same can be stated at the edges of $\mathcal{B}^*$.

Alternatively, $\operatorname{Im} E(\boldsymbol{k})$ may be *chosen* to be continuous in $\mathcal{B}^*$, in which case

$$E^*(-\boldsymbol{k}) = E(\boldsymbol{k}) \ . \tag{6.10}$$

The alternative between (6.9) and (6.10) is illustrated in Section 6.3. Thus, the band-dispersion functions possess either a symmetry or anti-symmetry, which are "inherited" from the $\mathcal{PT}$ symmetry of the potential.

Corrolary 1 (Symmetries of $E(\boldsymbol{k})$)**.** *The band-dispersion functions of Eq.* (5.1) *with a $\mathcal{PT}$-symmetric periodic potential* (6.1) *are either entirely real or form complex-conjugate pairs. Their real parts are continuous, even, and can be ordered in non-decreasing order* (6.4)*. Their imaginary parts can be chosen chosen to have even or odd symmetries. In particular,*

1. *Even symmetry* (6.10). *This implies that* $\boldsymbol{k} \mapsto \operatorname{Im} E_j(\boldsymbol{k})$ *is continuous. Moreover, for any two complex-conjugate band-dispersion functions, their imaginary parts can be ordered in non-decreasing order.*

2. *Odd or* $\mathcal{PT}$ *symmetry* (6.9). *This choice can result in band-dispersion functions that have discontinuous imaginary parts at the origin and / or the edges of the Brillouin zone.*

6.2 Perturbation analysis at exceptional points

In analogy to the real-potential case, two sequential band-dispersion functions are said to have a spectral gap if

$$\max_{\boldsymbol{k}} \operatorname{Re} E_j(\boldsymbol{k}) < \min_{\boldsymbol{k}} \operatorname{Re} E_{j+1}(\boldsymbol{k}) \ .$$

An exceptional point $\boldsymbol{k}_\star$ arising from a small perturbation of a direct gap occurs when

$$\operatorname{Re} E_j(\boldsymbol{k}_\star) = \operatorname{Re} E_{j+1}(\boldsymbol{k}_\star) \ .$$

What happens to the band-dispersion functions at an exceptional point under a small perturbation? For non-periodic potentials an analogous question was addressed in [62, 63, 55]. The analysis for periodic potentials is similar, but there are different consequences in the periodic case. In particular, we show that for complex $\mathcal{PT}$-symmetric potentials, the band-dispersion functions become complex following the closure of a spectral gap.

We define a *critical potential*, $V_{\rm cr}(\boldsymbol{x})$, as a potential for which two (sequential) band-dispersion functions have the same (real) value at an exceptional point $\boldsymbol{k}_\star$, *i.e.*, for some $j \in \mathbb{N}$ (and for no other values of j),

$$\lambda = E_j(\boldsymbol{k}_\star; 0) = E_{j+1}(\boldsymbol{k}_\star; 0) \in \mathbb{R} \ . \tag{6.11}$$

For $\mathcal{PT}$-symmetric problems, it has been shown that the transition from real to to complex spectra generically occurs when the imaginary part of the potential is greater than some non-zero threshold [42, 65, 11, 64, 19, 17]. Thus, $V_{\rm cr}(\boldsymbol{x})$ has a non-zero imaginary part.

Consider the perturbed potential

$$V(\boldsymbol{x}; \epsilon) = V_{\rm cr}(\boldsymbol{x}) + \epsilon^2 V_{\rm pert.}(\boldsymbol{x}) \ , \tag{6.12}$$

where $0 < \epsilon \ll 1$. Thus, Eq. (5.3) becomes

$$\Big[-(\nabla + i\mathbf{k})^2 + V_{\rm cr} + \epsilon^2 V_{\rm pert.}(bx) \Big] p(\boldsymbol{x}, \boldsymbol{k}; \epsilon) = E(\boldsymbol{k}; \epsilon) p(\boldsymbol{x}, \boldsymbol{k}; \epsilon) \ . \tag{6.13}$$

The two band functions and their corresponding Bloch eigenfunctions are expanded as at the exceptional point as

$$E_j(\boldsymbol{k}_\star; \epsilon) = \lambda + \epsilon E_j^{(1)}(\boldsymbol{k}_\star) + \epsilon^2 E_j^{(2)}(\boldsymbol{k}_\star) + \ ... \tag{6.14}$$

$$p_j(\boldsymbol{x}, \boldsymbol{k}_\star; \epsilon) = p_j^{(0)}(\boldsymbol{x}; \boldsymbol{k}_\star) + \epsilon p_j^{(1)}(\boldsymbol{x}; \boldsymbol{k}_\star) + \epsilon^2 p_j^{(2)}(\boldsymbol{x}; \boldsymbol{k}_\star) + \ ... \tag{6.15}$$

A couple of remarks are in order.

1. The choice of ϵ^2 in (6.12), compared with the (seemingly regular) expansion (6.14) is due to the second-order degeneracy at the degenerate point $\boldsymbol{k}_\star$ (see additional remarks at the end of this section).

2. $V_{\rm cr}(\boldsymbol{x})$ is $\mathcal{PT}$-symmetric , but there is no such stipulation $V_{\rm pert.}(\boldsymbol{x})$ at this point.

   It is expedient to define

$$\mathcal{L}_0 \doteq -(\nabla + i\boldsymbol{k}_\star)^2 + V_{cr} - \lambda \ . \tag{6.16}$$

Substituting (6.14) into (6.13) gives

$$\mathcal{O}(1): \quad \mathcal{L}_0 p_j^{(0)}(\boldsymbol{x},\boldsymbol{k}_\star) = 0 \ , \tag{6.17}$$

$$\mathcal{O}(\epsilon): \quad \mathcal{L}_0 p_j^{(1)}(\boldsymbol{x};\boldsymbol{k}_\star) = E_j^{(1)} p_j^{(0)}(\boldsymbol{x};\boldsymbol{k}_\star) \ , \tag{6.18}$$

$$\mathcal{O}(\epsilon^2): \quad \mathcal{L}_0 p_j^{(2)}(\boldsymbol{x};\boldsymbol{k}_\star) = E_j^{(1)} p_j^{(1)}(\boldsymbol{x};\boldsymbol{k}_\star) + \left[E_j^{(2)} - V_{\rm pert.}(\boldsymbol{x})\right] p_j^{(0)}(\boldsymbol{x};\boldsymbol{k}_\star) \tag{6.19}$$

Equation (6.17) has two linearly independent solutions. However, because of the second-order degeneracy of λ, there is a generalized Bloch eigenfunction, $q_j(\boldsymbol{x},\boldsymbol{k}_\star)$, such that

$$\mathcal{L}_0 q_j(\boldsymbol{x},\boldsymbol{k}_\star) = p_j^{(0)}(\boldsymbol{x},\boldsymbol{k}_\star) \ . \tag{6.20}$$

It follows from the $\mathcal{PT}$ symmetry (6.3), that the solution of the adjoint problem to (6.17) is $p_j^{(0)}(-\boldsymbol{x},\boldsymbol{k}_\star)$. Therefore, using the solvability condition for (6.20) and (6.3) yields

$$\int p_j^{(0)}(\boldsymbol{x},\boldsymbol{k}_\star)\left[p_j^{(0)}(-\boldsymbol{x},\boldsymbol{k}_\star)\right]^* d\boldsymbol{x} = \int \left[p_j^{(0)}(\boldsymbol{x},\boldsymbol{k}_\star)\right]^2 d\boldsymbol{x} = 0 \ . \tag{6.21}$$

Imposing the solvability condition on (6.18) and using (6.21) shows that $E_j^{(1)}$ is not determined at this order. However, using (6.20) and (6.18) one has

$$p_j^{(1)}(\boldsymbol{x};\boldsymbol{k}_\star) = E_j^{(1)} q_j^{(0)}(\boldsymbol{x};\boldsymbol{k}_\star) \ . \tag{6.22}$$

Imposing the solvability condition on (6.19), using (6.21) and (6.3) leads to

$$\left[E_j^{(1)}\right]^2 = \frac{\displaystyle\int V_{\rm pert.}(\boldsymbol{x})\left[p_j^{(0)}(\boldsymbol{x},\boldsymbol{k}_\star)\right]^2 d\boldsymbol{x}}{\displaystyle\int q_j(\boldsymbol{x};\boldsymbol{k}_\star) p_j^{(0)}(\boldsymbol{x},\boldsymbol{k}_\star)\, d\boldsymbol{x}} \ . \tag{6.23}$$

At the exceptional point, this quantity is independent of which of the two band-dispersion functions is chosen. For this reason, we denote

$$\beta = \left[E^{(1)}\right]^2 = \frac{\displaystyle\int V_{\rm pert.}(\boldsymbol{x})\left[p^{(0)}(\boldsymbol{x},\boldsymbol{k}_\star)\right]^2 d\boldsymbol{x}}{\displaystyle\int q(\boldsymbol{x};\boldsymbol{k}_\star) p^{(0)}(\boldsymbol{x},\boldsymbol{k}_\star)\, d\boldsymbol{x}} \ . \tag{6.24}$$

It follows from (6.24) and the symmetry analysis in Section 6.1 that the two band-dispersion functions form a complex-conjugate pair if and only if $\beta < 0$. This shows, in a perturbative sense, that the closure of a direct spectral gap directly follows the formation of a degenerate point in the band-dispersion functions.

We remark that β can also be written in two other ways,

$$\beta = \left[\frac{dE(\boldsymbol{k};\epsilon)}{d\epsilon}\right]^2 = \frac{\langle V_{\text{pert.}}(\boldsymbol{x}) p_j^{(0)}(\boldsymbol{x};\boldsymbol{k}_\star), p_j^{(0)}(\boldsymbol{x};\boldsymbol{k}_\star)\rangle_{\mathcal{PT}}}{\langle q_j(\boldsymbol{x};\boldsymbol{k}_\star), p_j^{(0)}(\boldsymbol{x},\boldsymbol{k}_\star)\rangle_{\mathcal{PT}}} \ . \tag{6.25}$$

The former follows from the perturbation expansion (6.14), while the later uses the $\mathcal{PT}$ inner-product defined as [25, 23]

$$\langle f(\boldsymbol{x}), g(\boldsymbol{x})\rangle_{\mathcal{PT}} \ = \ \int_{\mathcal{B}} f(\boldsymbol{x}) g^*(-\boldsymbol{x})\, d\boldsymbol{x} \ . \tag{6.26}$$

6.2.1 The sign of β and irreversibility

In general, β [Eq. (6.24)] can be complex. Here we determine *a-priori* that $\beta < 0$ for a special class of perturbations. Let $V_{\text{cr}}(\boldsymbol{x}) = V_R(\boldsymbol{x}) + iV_I(\boldsymbol{x})$ be a critical potential and consider the perturbed potential

$$V(\boldsymbol{x};\epsilon) = V_{\text{cr}}(\boldsymbol{x}) + i\epsilon^2 V_I(\boldsymbol{x}) = V_R(\boldsymbol{x}) + i(1+\epsilon^2)V_I(\boldsymbol{x}) \ . \tag{6.27}$$

Thus, $V_{\text{pert.}}(\boldsymbol{x}) \equiv iV_I(\boldsymbol{x})$ is an odd (and $\mathcal{PT}$-symmetric) function. First, we show that β is real. We denote the numerator and denominator of β respectively by

$$\nu \ = \ \int V_{\text{pert.}}(\boldsymbol{x}) \left[p_j^{(0)}(\boldsymbol{x},\boldsymbol{k}_\star)\right]^2 d\boldsymbol{x} \ , \tag{6.28}$$

$$D \ = \ \int q_j(\boldsymbol{x};\boldsymbol{k}_\star) p_j^{(0)}(\boldsymbol{x},\boldsymbol{k}_\star)\, d\boldsymbol{x} \ . \tag{6.29}$$

Since $p_j^{(0)}(\boldsymbol{x},\boldsymbol{k}_\star)$ is $\mathcal{PT}$-symmetric , it can be chosen such that its real and imaginary parts are even and odd, respectively. That D is real follows from the $\mathcal{PT}$ symmetry of $p_j^{(0)}$ and of q_j, the latter resulting from (6.20). In addition, it follows from (6.27) and the $\mathcal{PT}$ symmetry of $p_j^{(0)}$ that

$$\nu = -\int V_I(\boldsymbol{x}) \operatorname{Re} p_j^{(0)}(\boldsymbol{x},\boldsymbol{k}_\star) \operatorname{Im} p_j^{(0)}(\boldsymbol{x},\boldsymbol{k}_\star)\, d\boldsymbol{x} \ . \tag{6.30}$$

Hence, both ν and $\beta = \nu/D$ are real.

We claim that, for (6.27), $\operatorname{sign}\nu = -\operatorname{sign} D$. To see why, consider the "reversed" perturbation, $V_{\text{pert.}} = -iV_I$. Because V_{cr} is critical, this "reversed" perturbation ensures that, for $0 \le \epsilon \ll 1$, there are be two real and distinct band-dispersion functions. This implies that $\beta > 0$ and, therefore, $\operatorname{sign}\nu = \operatorname{sign} D$. Flipping back the sign of the perturbation yields $\operatorname{sign}\nu = -\operatorname{sign} D$. We conclude that $\beta = \nu/D < 0$.

Corrolary 2 (Irreversibility)**.** *For the class of potentials* (6.27)*, $\beta < 0$. As ϵ increases, the band dispersion functions transition from real to complex conjugates.*

This corresponds to irreversibility in the sense that there is a definite "direction" in which the imaginary part of the perturbation affects the real parts of the band-dispersion functions. We elucidate this using computations in the next sections. Irreversibility is related to other phenomena that have been studied in $\mathcal{PT}$-symmetric systems, such as hysteresis [62], non-reciprocity [50, 49], and jamming anomaly [9].

6.2.2 Generalizations of the perturbation analysis

The perturbation analysis above can be readily generalized to the following cases.

1. Multiple exceptional points.
2. When more than two band-dispersion functions coalesce at the same exceptional point.

The former is straightforward. For the latter, assume $m \in \mathbb{N}$ band-dispersion functions coalesce at $\boldsymbol{k}_\star$. Setting $V(\cdot;\epsilon) = V_{\rm cr} + \epsilon^m V_{\rm pert.}$, the perturbation analysis would proceed to order $\mathcal{O}(\epsilon^m)$ and would need to distinguish between various cases, which depend on the degree to which the degeneracy is removed by the perturbation.

6.3 Computations of band-dispersion functions

To elucidate the analytical results, we compute them for a one-parameter family of problems. Specifically, we consider Eq. (5.1) in one-dimension with the $\mathcal{PT}$-symmetric potential

$$V(x) = \cos^2(x) \; + \; iW_0 \sin(2x) \; , \tag{6.31}$$

where the parameter W_0 varies. The fundamental cell is $\mathcal{B} = [-\frac{\pi}{2}, \frac{\pi}{2}]$ and the first Brillouin zone is $\mathcal{B}^* = [-1, 1]$.

Figure 6.1 presents the minima and maxima of the real parts of the first four band-dispersion functions, *i.e.*, $\min_{k\in\mathcal{B}^*} E_j(k;W_o)$ and $\max_{k\in\mathcal{B}^*} E_j(k;W_0)$ for $j = 1..4$, as W_0 varies. The points designated by A – C in Fig. 6.1 are discussed below. Figures 6.2–6.4 present the real and imaginary parts of the band-dispersion functions for various values of W_0. We make several observations based on these computations.

1. For $W_0 \leq 0.5$ all the band-dispersion functions are real. There is a direct gap between E_1 and E_2 at the edges of the Brillouin zone, see Fig. 6.2(a1).

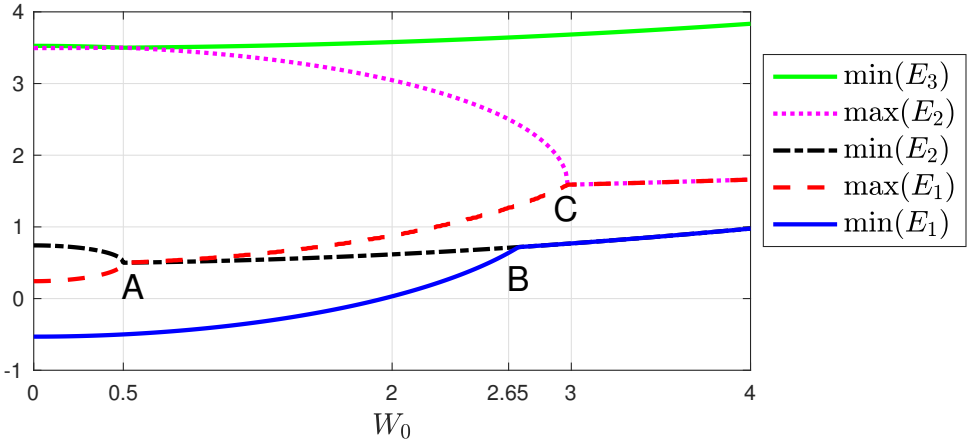

Figure 6.1: The real parts of the first few band-dispersion functions corresponding to the potential (6.31) as a function of W_0.

2. At $W_0 = 0.5$ (Point A), $E_1(k)$ and $E_2(k)$ merge at the edges of the Brillouin zone. See Fig. 6.2(b1). This is the first closure of a spectral gap as W_0 is increasing.

3. For $W_0 > 0.5$, $E_1(k)$ and $E_2(k)$ become complex conjugates, see Fig. 6.3. Their real parts merge from the edges of the Brillouin zone inward, *i.e.*,

$$\operatorname{Re} E_1(k) = \operatorname{Re} E_2(k) \ , \quad \forall |k| > k_{\rm cr}(W_0) \ ,$$

where $W_0 \mapsto k_{\rm cr}(W_0)$ is a non-increasing function.

4. At $W_0 \approx 2.65$ (Point B), $\min \operatorname{Re} E_1 = \min \operatorname{Re} E_2$ (see Fig. 6.3). As W_0 increases above this value, the location of the minimum of $E_1(k)$ changes abruptly from the edges of the Brillouin zone to its origin. Thus, $W_0 \mapsto \arg\min_k \operatorname{Re} E_1(k; W_0)$ is not C^1, which explains the sharp transition at Point B in Fig. 6.1.

5. At $W_0 = 3$ (Point C), $\operatorname{Re} E_1(k) \equiv \operatorname{Re} E_2(k)$, *i.e.*, the real parts of these two band-dispersion functions have completely coalesced. See Fig. 6.4(a1,a2).

6. Figure 6.1 shows that, as W_0 increases, the real parts of sequential band-dispersion functions can coalesce, but do not bifurcate. This is a manifestation of Corollary 2 and irreversibility discussed in Section 6.2.1.

Figures 6.5 and 6.6 present the imaginary parts of the first two the band-dispersion functions when they are replicated over the adjacent Brillouin zones. These two figures demonstrate the alternative between even and odd symmetries of the imaginary parts as discussed in Section 6.1. Mathematically, the even symmetry is preferable, since the resulting imaginary parts are continuous

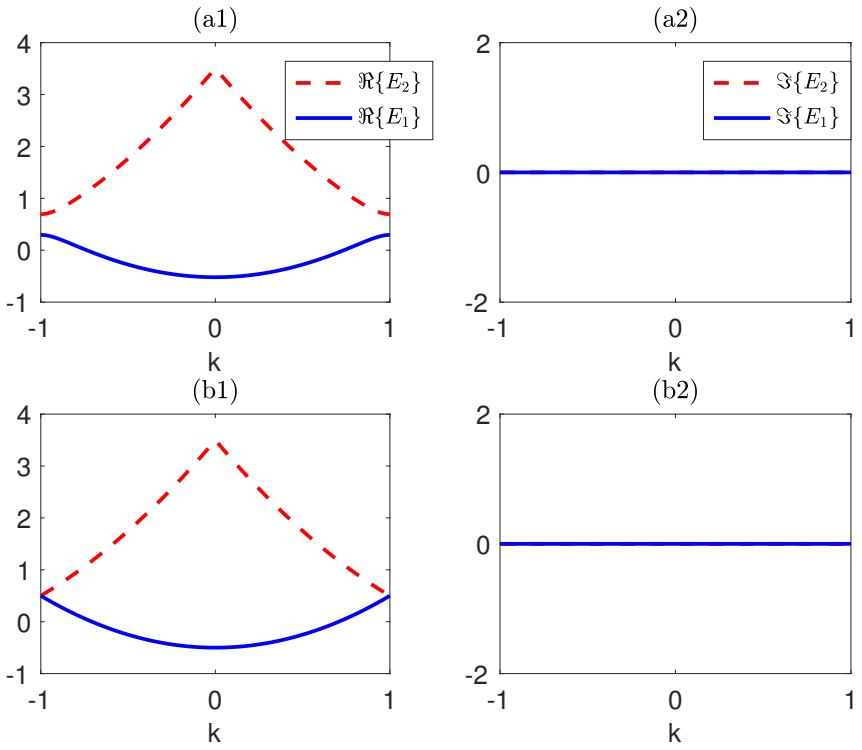

Figure 6.2: The first two band dispersion functions of Eq. (5.3) with the potential (6.31) and (a1 & a2) $W_0 = 0.3$ (b1 & b2) $W_0 = W_{cr} = 0.5$. The real and imaginary parts are shown on the left and right panels, respectively. Here, the imaginary parts are identically zero.

and can be ordered in non-decreasing values. Physically, the odd symmetry "inherits" the $\mathcal{PT}$ symmetry , which is interesting. However, as Fig. 6.6 shows, the imaginary parts of the band-dispersion functions are discontinuous – in this case at the edges of the Brillouin zone. In some sense, it can be said that complex-conjugate band-dispersion functions are part of the same spectral band, in which case the notation (6.5) may be useful.

6.4 Highly-localized perturbations

It is interesting to study the effect of highly-localized perturbations on the exceptional points. To do so, we consider the one-parameter family of perturbed

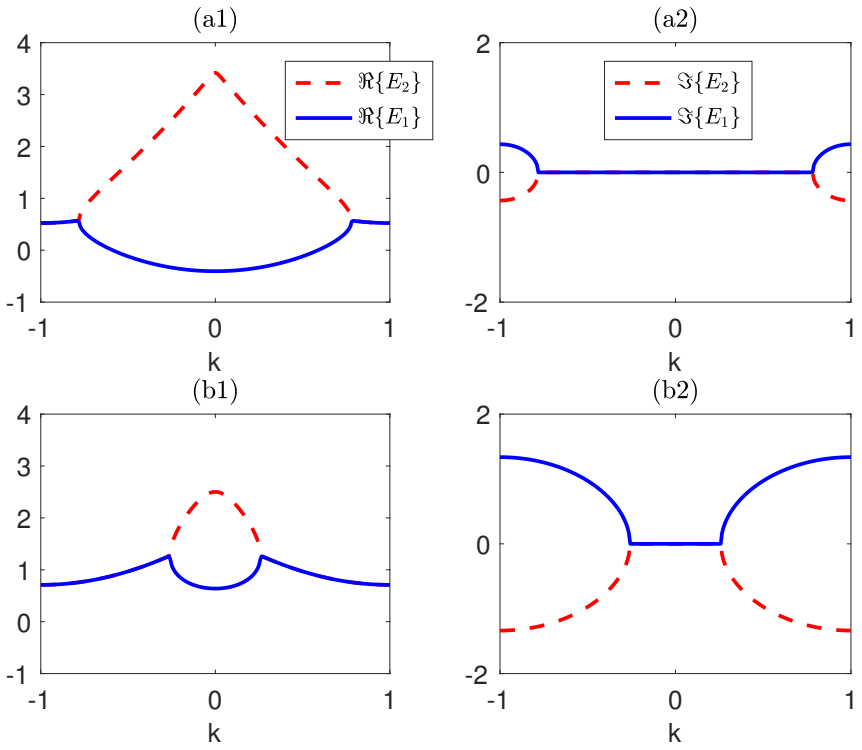

Figure 6.3: Same as Fig. 6.2 with (a1 & a2) $W_0 = 1$; (b1 & b2) $W_0 = 2.65$. The imaginary parts form a complex conjugate pair of continuous and even functions.

$\mathcal{PT}$ symmetry potentials

$$V(x;P) = V_{\rm cr}(x) + V_{\rm pert.}(x;P) \ , \tag{6.32a}$$

$$V_{\rm cr}(x) = \cos^2(x) + \frac{i}{2}\sin(2x) \ , \tag{6.32b}$$

$$V_{\rm pert.}(x;P) = i\sin^P(2x) \ , \tag{6.32c}$$

where where P is an odd integer. Here $V_{\rm cr}(x)$ is the potential (6.31) at the critical parameter $W_0 = 0.5$, at which the gap between the two band-dispersion functions closes. We note that $V_{\rm pert.}(x;P)$ is not a small perturbation. However, as P increases, $V_{\rm pert.}(x;P)$ becomes more localized at the points $x = \pm\frac{\pi}{2}$.

We are interested in the behavior of β [Eq. (6.24)] for large values of P. Since the denominator of β [Eq. (6.29)] is independent of the perturbation $V_{\rm pert.}$, we focus on the numerator (6.30). It follows from the $\mathcal{PT}$ symmetry of

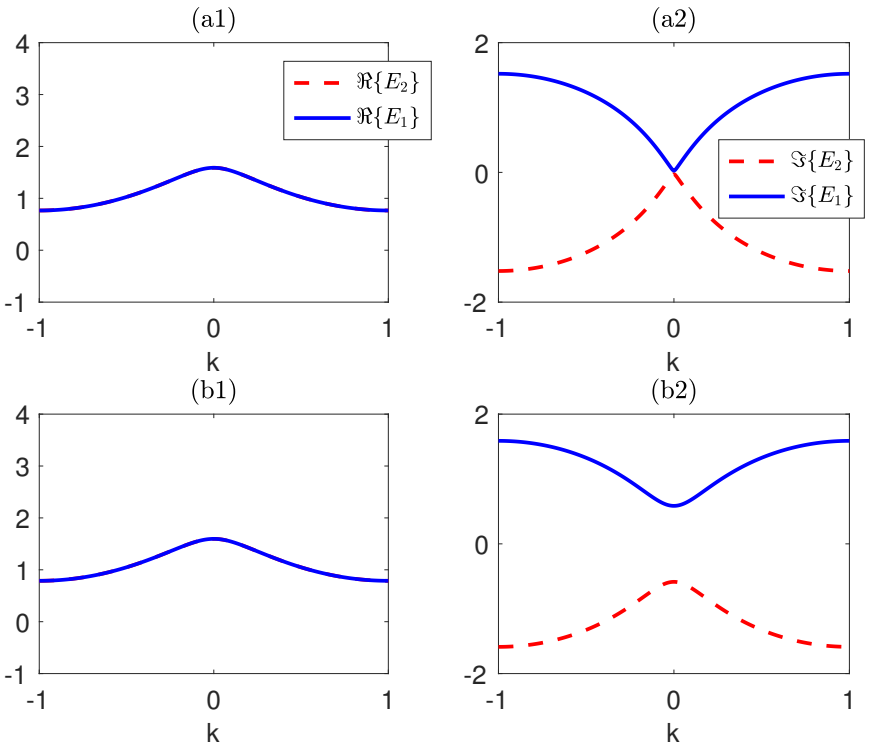

Figure 6.4: Same as Fig. 6.3 with (a1 & a2) $W_0 = 2.98$; (b1 & b2) $W_0 = 3.1$.

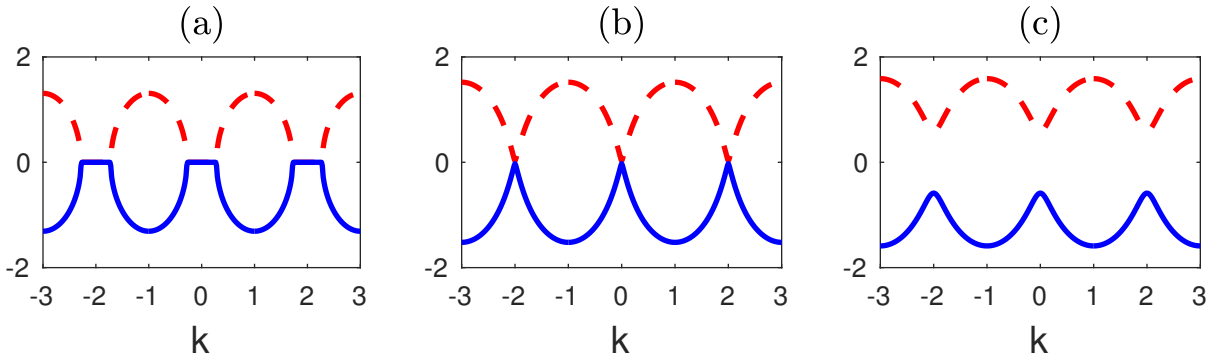

Figure 6.5: The imaginary parts of the first two band-dispersion functions continued periodically to the adjacent Brillouin zones corresponding to the potential (6.31) with (a) $W_0 = 2.6$; (b) $W_0 = 2.98$; and (c) $W_0 = 3.1$. Here the imaginary parts are chosen as even, They are are continuous in $\mathcal{B}^*$ and can be ordered in non-decreasing values.

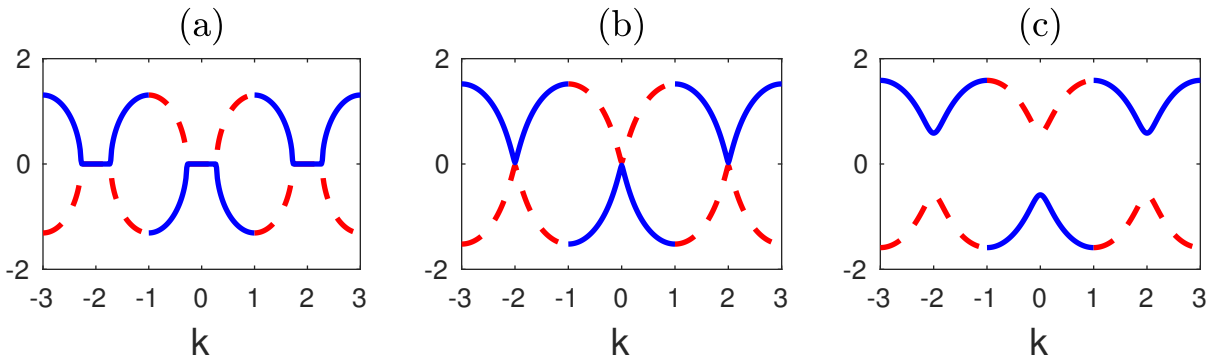

Figure 6.6: Same as Fig. 6.51, but with the imaginary parts chosen as odd functions. In this case, they are discontinuous at the edges of Brillouin zone, *i.e.*, at $k = \pm 1, \pm 3, \ldots$.

$x \mapsto p_j^{(0)}(x, k_\star)$ that the numerator can be written as

$$\nu(P) = \int_{-\pi/2}^{\pi/2} \sin^P(2x) f(x)\, dx \ , \tag{6.33}$$

where we have defined

$$f(x) = \mathrm{Re}\, p^{(0)}(x, k_\star)\, \mathrm{Im}\, p^{(0)}(x, k_\star) \ . \tag{6.34}$$

It follows from the $\mathcal{PT}$ symmetry of $p^{(0)}(x, k_\star)$ that $f(x)$ is an odd function. In 6.5.1 we show that

$$\nu(P) \ \sim \ \frac{C}{\sqrt{P}} \quad \text{as } P \to \infty \ . \tag{6.35}$$

where $C = 4\sqrt{\pi} f(\pi/4)$. Consequently,

$$\beta(P) \ \sim \ \frac{C_1}{\sqrt{P}} \quad \text{as } P \to \infty \ . \tag{6.36}$$

where C_1 is a constant.

6.5 Numerical validation of the perturbation and asymptotic results

In this section we validate numerically the results of the perturbation analysis in Section 6.2 and asymptotic analysis in Section 6.4.

To validate the perturbation analysis, we choose a small perturbation of the same critical potential as in Section 6.4, *i.e.*,

$$V(x;P,\epsilon) = V_{\rm cr}(x) + \epsilon^2 V_{\rm pert.}(x;P) \ , \tag{6.37a}$$

$$V_{\rm cr}(x) = \cos^2(x) + \frac{i}{2}\sin(2x) \ , \tag{6.37b}$$

$$V_{\rm pert.}(x;P) = i\sin^P(2x) \ , \tag{6.37c}$$

where $0 < \epsilon \ll 1$. In the computations we have used $\epsilon = 0.01$.

We need to compute the quantity β, Eq. (6.24). While it is possible to do so it using (6.24), evaluating the denominator requires solving (6.20), which is highly ill-posed. Instead, we estimate β directly as follows. Let $E_j(k_\star;\epsilon), j = 1,2$, denote the first two band-dispersion functions corresponding to the potential (6.37). At $\epsilon = 0$, the gap closes at $k_\star = \pm 1$ [see Fig. 6.2]. Therefore, $\beta < 0$ and the band dispersion functions become complex conjugates at $k_\star$ for $\epsilon > 0$. Using (6.25), β can be numerically approximated by

$$\beta \approx \left[\frac{E_1(k_\star;\epsilon) - E_1(k_\star;0)}{\epsilon}\right]^2 \ , \tag{6.38}$$

Figure 6.7(a) shows that the value of β computed using the perturbation analysis (6.24) is almost indistinguishable from the numerical approximation using (6.38).

To validate numerically the asymptotic result in Section 6.4, we use the same numerical procedure. Figure 6.7(b) shows that the value of β computed using (6.36) is very close to the numerical approximation (6.38) for $P \geq 10$.

6.5.1 Asymptotics for the integral (6.33)

To obtain the large-P behavior of $\nu(P)$ in (6.33), we first transform the variables to obtain a Laplace-type integral. This is done in two stages. First, we consider the interval $x \in [\pi/4, \pi/2)$. In this interval, $\sin^P(2x)$ is monotonically decaying. Thus, we make the 1-to-1 transformation $x \mapsto u(x)$, such that $e^{-u} = \sin(2x)$. This yields

$$\nu_r(P) = \frac{1}{2}\int_0^\infty \frac{h(u)e^{-u}}{\sqrt{1-e^{-2u}}} e^{-Pu}\, du$$

where $h(u) = f(\frac{1}{2}\sin^{-1} e^u)$ and $f(x)$ is given by (6.34). Using Watson's Lemma [6], to leading order

$$\nu_r \sim h(0)\sqrt{\frac{\pi}{P}} \quad \text{as } P \to \infty \ .$$

As $\sin^P(2x)$ is locally even around $x = \pm\frac{\pi}{4}$, the entire contribution of this point to $\nu(P)$ is $2\nu_r$. The odd symmetries of $\sin^P(2x)$ and $h(x)$ about $x = 0$ give

$$\nu \sim 4h(0)\sqrt{\frac{\pi}{P}} \quad \text{as } P \to \infty \ .$$

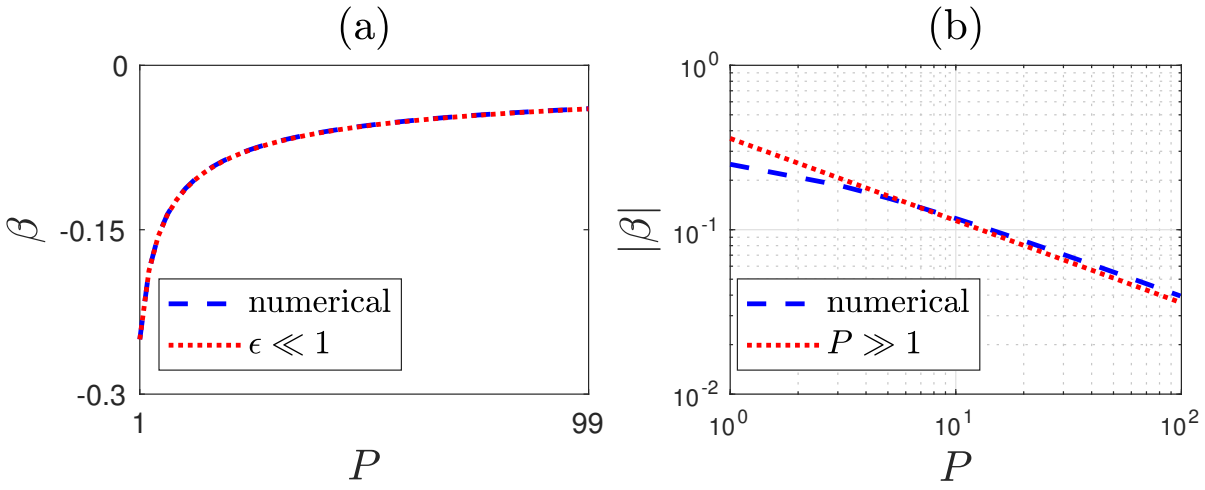

Figure 6.7: (a) The ratio β [Eq. (6.24)] computed using the perturbation analysis (6.24) and using the numerical approximation (6.38) for the potential (6.37) as a functions of the odd exponent P. (b) Same problem as (a) showing the log-log plot of $|\beta|$ obtained using the large-P asymptotics (6.36) compared with the numerical approximation (6.38).

Using $h(0) = f(\pi/4)$ yields (6.35).

6.6 Summary and conclusions

The main results of this study are summarized in Corollaries 1 and 2. In particular, symmetry analysis shows that the imaginary parts of the the band-dispersion functions can be chosen as even, which is mathematically advantageous to to continuity, or as odd, in which case the band-dispersion functions "inherit" the $\mathcal{PT}$ symmetry , but can be discontinuous. We establish that the band-dispersion functions become complex following the closure of a spectral gap at an exceptional (degenerate) point. In addition, asymptotic analysis reveals that the rate of change of the the band-dispersion functions is reduced as the perturbation becomes more localized [Eq. (6.36)]. These results shed new light on the irreversible nature of the phase transition in $\mathcal{PT}$-symmetric systems, which have garnered much interest due to their fascinating mathematical and physical properties.

Appendix

Appendix A

Hamiltonian of Dipolar NLS Equation

A.1 Hamiltonian Calculation

Calculation of the Hamiltonian for the NLS Equation with dipolar interactions.

$$i\hbar\psi_t + \frac{\hbar^2}{2}\Delta\psi - V\psi - g_1|\psi|^2\psi - g_2 V_{\text{dip}}\left(|\psi|^2\right)\psi = 0 \tag{A.1}$$

Multiplying by ψ_t^* and adding the complex conjugate of the system returns

$$\begin{aligned} &i\hbar\left(\psi_t^*\psi_t - \psi_t\psi_t\right) + \frac{\hbar^2}{2}\left(\psi_t^*\Delta\psi + \psi_t^*\Delta\psi^*\right) - V\left(\psi\psi_t^* + \psi^*\psi_t\right) \\ &- g_1|\psi|^2\left(\psi\psi_t^* + \psi^*\psi_t\right) - g_2 V_{\text{dip}}\left(|\psi|^2\right)\left(\psi\psi_t^* + \psi^*\psi_t\right) = 0 \end{aligned} \tag{A.2}$$

Simplification yields

$$\frac{\hbar^2}{2}\left(\psi_t^*\Delta\psi + \psi_t\Delta\psi^*\right) - \frac{\partial}{\partial t}\left(|\psi|^2\right)\left(V + g_1|\psi|^2 + g_2 V_{\text{dip}}\left(|\psi|^2\right)\right) = 0. \tag{A.3}$$

Let us look at the nonlinear terms individually. From the cubic nonlinearity, we have

$$g_1\frac{\partial}{\partial t}\left(|\psi|^2\right)|\psi|^2.$$

We can rewrite this expression using the chain rule, such that

$$g_1\frac{\partial}{\partial t}\left(|\psi|^2\right)|\psi|^2 = \frac{g_1}{2}\frac{\partial}{\partial t}\left(|\psi|^4\right). \tag{A.4}$$

From the dipolar potential, we have

$$g_2\frac{\partial}{\partial t}\left(|\psi|^2\right)V_{\text{dip}}\left(|\psi|^2\right) = g_2\frac{\partial}{\partial t}\left(|\psi|^2\right)\int_{-\infty}^{\infty} U_{\text{dip}}(\mathbf{x}-\mathbf{x}')|\psi(\mathbf{x}',t)|^2 d\mathbf{x}'.$$

We have

$$V_{\text{dip}} = \frac{\partial}{\partial t}\left(|\psi(\mathbf{x},t)|^2\right)\int_{-\infty}^{\infty} U_{\text{dip}}(\mathbf{x}-\mathbf{x}')|\psi(\mathbf{x}',t)|^2 d\mathbf{x}'$$
$$= \int_{-\infty}^{\infty} U_{\text{dip}}(\mathbf{x}-\mathbf{x}')|\psi(\mathbf{x}',t)|^2 \frac{\partial}{\partial t}\left(|\psi(\mathbf{x},t)|^2\right) d\mathbf{x}' \tag{A.5}$$
$$\tag{A.6}$$

Assuming the mode $\psi(\mathbf{x},t)$ is symmetric,

$$V_{\text{dip}}(\mathbf{x},t) = \frac{1}{2}\int_{-\infty}^{\infty} U_{\text{dip}}(\mathbf{x}-\mathbf{x}')\frac{\partial}{\partial t}\left(|\psi(\mathbf{x}',t)|^2|\psi(\mathbf{x},t)|^2\right) d\mathbf{x}'$$
$$= \frac{\partial}{\partial t}\frac{1}{2}\int_{-\infty}^{\infty} U_{\text{dip}}(\mathbf{x}-\mathbf{x}')|\psi(\mathbf{x}',t)|^2|\psi(\mathbf{x},t)|^2 d\mathbf{x}'.$$

Let

$$\tilde{V}_{\text{dip}}(\mathbf{x},t) = \int_{-\infty}^{\infty} U_{\text{dip}}(\mathbf{x}-\mathbf{x}')|\psi(\mathbf{x}',t)|^2 d\mathbf{x}' \tag{A.7}$$

such that V_{dip} can be rewritten as

$$V_{\text{dip}}(\mathbf{x},t) = \frac{1}{2}\frac{\partial}{\partial t}|\psi(\mathbf{x},t)|^2\tilde{V}_{\text{dip}}(\mathbf{x},t).$$

After one integration by parts and plugging in our new expressions for the cubic and dipolar nonlinearities, we integrate Eq.(A.3) with respect to $\mathbf{x}$. This integration returns

$$\frac{\partial}{\partial t}\int_{\mathbb{R}^3} -\frac{\hbar^2}{2}|\nabla\psi(\mathbf{x},t)|^2 - V|\psi(\mathbf{x},t)|^2 - \frac{g_1}{2}|\psi(\mathbf{x},t)|^4 - \frac{g_2}{2}\tilde{V}_{\text{dip}}(\mathbf{x},t)|\psi(\mathbf{x},t)|^2 d\mathbf{x} = 0.$$

This gives us the Hamiltonian of the system

$$\mathcal{H} = \int_{\mathbb{R}^3} \hbar^2|\nabla\psi|^2 + 2V|\psi|^2 + g_1|\psi|^4 + g_2\tilde{V}_{\text{dip}}|\psi|^2 d\mathbf{x} = \mathcal{C}$$

where $\mathcal{C}$ is a constant.

A.2 Numerical Implementation

```
% Constants & Variables
h_mod      = hbar^2 / 2;
g1_mod     = g1 / 2;
g2_mod     = g2 / 2;

u_hat2     = DFTmat * |u|^2 * Hank';
u2         = |u|^2;
u4         = |u|^4;
```

```
Vu2        = V |u|^2;

% Potential Energy
PEng       = sum(sum(Vu2 .* R) .* dr .* dz);

% Kinetic Energies

% Laplacian
KEng_lap   = h_mod  .* sum(sum((K2 .* u_hat2).* R)) .* ...
             dr .* dz./ (Nr.*Nz);
% Cubic Nonlinearity
KEng_cub   = (g1_mod - g2_mod).* ...
             sum(sum(u4 .* R)) .* dr .* dz;
% Dipolar Interactions
KEng_dip   = 3 .* g2_mod .* sum(sum(((KR .*KZ).^2 .* ...
             abs((DFTmat * varphi * Hank')).^2) .* KR)) .* ...
             dkr .* dkz ./ (Nr.*Nz.^2);

% Total Energy of the System
Hamil      = PEng + KEng_lap + KEng_cub + KEng_dip;
% Absolute Values of Energy Contributions
Hamil_sum = |PEng| + |KEng_lap| + |KEng_cub| + |KEng_dip|;


Hamil_sum = max(Hamil_sum);
```

Appendix B

Accelerated Imaginary-Time Evolution (A-ITEM):

B.1 Detail of Method

The Accelerated Imaginary-Time Evolution Method (A-ITEM) is a gradient descent method. A-ITEM is used to numerically approximate ground states of the NLS equation. By adding a preconditioner to the original ITEM, Yang and Lakoba developed A-ITEM [75]. There exist two types: 1) L_2 normalization and 2) amplitude normalization.

A-ITEM with L_2 (power) normalization is a natural extension for ITEM. The user prescribes an L_2 norm value for which the solution will be iteratively scaled so that it has that L_2 norm. With L_2 normalization, the method quickly converges to a suitable ground state. However, the method is sensitive to the V.K. stability criterion,

$$P'(\mu) < 0$$

where P is the L_2 norm of the ground state and μ is the associated frequency obtained from the stationary equation. For $P'(\mu) = 0$, it is known that A-ITEM with L_2 normalization behaves catastrophically.

However, A-ITEM with amplitude normalization is not sensitive to the V.K. condition. Here, the user prescribes an amplitude for which the solution will be iteratively scaled to possess. The method will converge regardless of the stability of the system. In our work, we choose to implement A-ITEM with amplitude normalization.

Imaginary-Time Evolution Methods (ITEM) have been around for a long time. The idea behind ITEM is that we make the transformation $it \to t$ and solve the problem with a gradient descent method. Between each iteration of the method we will normalize the method such that the solution has either a

fixed L_2 norm or amplitude.

To implement this method, we work with both the time-dependent and stationary NLS equations, respectively,

$$\begin{cases} i\psi_t &= -\frac{\hbar^2}{2m}\Delta\psi + V\psi + |\psi|^2\psi \\ \mu u &= -\Delta u + Vu + |u|^2 u \end{cases} \tag{B.1}$$

where $\psi(x, y, t) = u(\mathbf{x}) \exp(-i\mu t)$, parametrized by the frequency μ. System (B.1) can be written as

$$\begin{cases} \psi_t &= L_{00}\psi \\ \mu u &= L_{00} u \end{cases} \tag{B.2}$$

respectively.

In A-ITEM, by letting $it \to t$, we simply iterate

$$u_t = L_{00} u$$

then normalize the solution of each iteration by a fixed L_2 norm (power) or amplitude. By eye and definition of gradient descent methods, it may appear that by desiring $u_t \to 0$, we are forcing $\mu \to 0$. Computationally, this is not the case because we are continuously normalizing the solution to have a fixed positive L_2 norm or amplitude. Since $\mu = 0$ corresponds to $u = 0$ this would imply that $\langle u, u\rangle_2 = 0$, which is forbidden. Therefore, A-ITEM will converge to a non-zero solution with a non-zero frequency μ.

ITEM converges to an accurate solution to the stationary equation. However, it is known to do so slowly. The main goal of A-ITEM is to speed up the convergence rate of the pre-existent ITEM. This is done by adding a preconditioner to the system (B.1), such that the system

$$\begin{cases} u_t &= M^{-1}[L_{00} - \mu]u \\ \mu &= \langle L_{00}u, M^{-1}u\rangle_2 / \hbar\langle u, M^{-1}u\rangle_2 \end{cases} \tag{B.3}$$

is obtained, where $\langle f, g\rangle_2$ represents the L_2 norm.

B.1.1 Amplitude Normalization:

A-ITEM with "non-traditional amplitude normalization" delivers better results than A-ITEM with standard L_2 normalization. Here, the amplitude of the solution is fixed to be the user-prescribed value whilst we iterate. The benefit of amplitude normalization lies in the independency from the V.K. stability criterion. A-ITEM with L_2 normalization requires that we be cognicent of the rate of change of the L_2 norm with respect to μ, such that

$$P'(\mu) < 0$$

where P is the L_2 norm of the solution. Here, when $P'(\mu) = 0$, A-ITEM with power normalization will fail. However, A-ITEM with amplitude normalization does not care and does not require this at all. A-ITEM with amplitude normalization will converge regardless.

Addition of the amplitude normalization into A-ITEM returns the following scheme

$$\begin{cases} u_t &= M^{-1}[L_{00} - \mu]u \\ u &= A(\max|u|)^{-1}u \\ \mu &= \langle L_{00}u, M^{-1}u\rangle_2 / \langle u, M^{-1}u\rangle_2 \end{cases} \tag{B.4}$$

B.2 Numerical Implementation

```
while residual > tol

        n     = n + 1;
        Uold  = U;
        L0OU  = epsilon^2*ifft(k2/2.*fft2(U)) + V.*U + g1*abs(U).^2.*U;
        MinvU = ifft(fft2(U).*DEN);
        mu    = real( trapz(x,L0OU.*MinvU)/trapz(x,U.*MinvU) ) / epsilon;
        U     = U + real( ifft(fft(L0OU - epsilon*mu*U).*DEN)*DT );
        L2    = trapz(x,U.*conj(U));

        residual(n) = max(abs(L0OU - epsilon*mu*U));

    switch NOR % Choice of either amplitude or L2 normalization
      case 'AMP'
        U       = U/max(abs(U(:)))*AMP;
      case 'L2'
        U       = U/sqrt(L2/P);
    end

end
```

Appendix C

Split-Step Fourier Transform (SSFT):

C.1 Detail of Method

Split-Step Fourier Transform (SSFT) routine is a pseudo-spectral – or Finite Fourier transform – method used to numerically approximate solutions on a finite spatial grid. Taha and Ablowitz [69] determined the SSFT to be the best method NLS equation soliton computation. For the implementation of this routine, we need the NLS equation,

$$iq\psi_t = -\psi_{xx} \pm |\psi|^2\psi, \tag{C.1}$$

where $\psi = \psi(x,t)$.

In order to implement the SSFT, we need to specify a periodic initial condition. Analytically, we will split the NLS equation into linear and nonlinear parts and solve each part independently. Numerically, we will alternately iterate these solutions in the SSFT routine.

We will now implement Strang splitting on Eq. (C.1).

C.1.1 Linear part: $i\psi_t = -\psi_{xx}$

Multiply the linear part by $-i$ and use Fourier Transforms (with respect to x):

$$\widehat{\psi}_t = i\widehat{\psi}_{xx} = -ik^2\widehat{\psi}, \tag{C.2}$$

where $\widehat{\psi} = \widehat{\psi(k,t)}$ and $\widehat{\psi}_0 = \widehat{\psi(k,0)}$. Separation of variables on Eq. (C.2) returns

$$\widehat{\psi}_{_L} = \widehat{\psi}_0 e^{-ik^2t} \tag{C.3}$$

and the inverse Fourier Transform of (C.3) yields

$$\psi_{_L} = \text{ifft}(\widehat{\psi}_0 e^{-ik^2t}). \tag{C.4}$$

C.1.2 Nonlinear part: $i\psi_t = -\psi|\psi|^2$

Multiply the nonlinear part by $-\psi^*$ and subtract the complex conjugate of the C.1 from the whole quantity, such that

$$\begin{aligned} i\left(\psi\psi_t^* + \psi^*\psi_t\right) &= 0 \\ &= \frac{\partial}{\partial_t}\left(\psi^*\psi\right) \\ &= \frac{\partial}{\partial_t}\left(|\psi|^2\right) \end{aligned} \tag{C.5}$$

This implies that $|\psi|^2 = |\psi_0(x)|^2$.

Now, we work with the equation

$$\psi_t = i|\psi_0|\psi \implies \psi_{NL} = \psi_0(x)e^{|\psi_0|t} \tag{C.6}$$

We will now alternately iterate these solutions in the SSFT routine.

C.2 Numerical Implementation

```
%For simplicity, let q = \psi

%Let q0 = sech(x/sqrt(2)) Nt = number of temporal points ep =
% dispersion-controlling factor

% First part of the split-step (dt/4; linear step)
q = ifft(fft(q0(x)).*exp(-(i)*ep*k.^(2)*(dt/4)));
E = exp((-i)*ep*k.^(2)*(dt/2));

%% Split-step loop: here, we alternately iterate between the linear
%% and nonlinear solutions

for j = 1:Nt
    q2 = q.*conj(q);
    % nonlinear part:
    q = exp((i/ep)*q2*(dt/2)).*q;
    if j < Nt
        % linear part:
        q = ifft(E.*fft(q));
    end
end
% Last part of the split-step (dt/4; linear step)
q = ifft(fft(q).*exp((-i)*ep*k.^(2)*(dt/4)));
```

Bibliography

[1] The Benney-Roskes / Davey-Stewartson system can be obtained from Eq. (3.7) by assuming that $\psi(\boldsymbol{r}, t)$ does not depend on x, $V_{\text{ext}} = 0$, and making the transformation $z \to x, y \to y$ and $\phi = \varphi_x$.

[2] F. K. Abdullaev, A. Gammal, B. A. Malomed, and L. Tomio. Bright solitons in quasi-one-dimensional dipolar condensates with spatially modulated interactions. *Physical Review A*, 87(6):063621, 2013.

[3] M. Ablowitz, İ. Bakırtaş, and B. Ilan. Wave collapse in a class of nonlocal nonlinear Schrödinger equations. *Physica D: Nonlinear Phenomena*, 207(3-4):230–253, 2005.

[4] M. J. Ablowitz, G. Biondini, and S. Blair. Multi-dimensional pulse propagation in non-resonant χ (2) materials. *Physics Letters A*, 236(5-6):520–524, 1997.

[5] M. J. Ablowitz, G. Biondini, and S. Blair. Nonlinear Schrödinger equations with mean terms in nonresonant multidimensional quadratic materials. *Physical Review E*, 63(4):046605, 2001.

[6] M. J. Ablowitz and A. S. Fokas. *Complex Variables: Introduction and Applications*. Cambridge University Press, 2003.

[7] M. H. Anderson, J. R. Ensher, M. R. Matthews, C. E. Wieman, and E. A. Cornell. Observation of Bose-Einstein condensation in a dilute atomic vapor. *Science*, 269(5221):198–201, 1995.

[8] M. A. Baranov. Theoretical progress in many-body physics with ultracold dipolar gases. *Physics Reports*, 464(3):71–111, 2008.

[9] I. Barashenkov, D. A. Zezyulin, and V. V. Konotop. Jamming anomaly in pt-symmetric systems. *New Journal of Physics*, 18(7):075015, 2016.

[10] G. Baruch and G. Fibich. Singular solutions of the l2-supercritical biharmonic nonlinear Schrödinger equation. *Nonlinearity*, 24(6):1843, 2011.

[11] C. M. Bender, M. Berry, and A. Mandilara. Generalized pt symmetry and real spectra. *Journal of Physics A: Mathematical and General*, 35(31):L467, 2002.

[12] C. M. Bender and S. Boettcher. Real spectra in non-hermitian hamiltonians having p t symmetry. *Physical Review Letters*, 80(24):5243, 1998.

[13] C. M. Bender and S. Boettcher. Real spectra in non-hermitian hamiltonians having pt symmetry. *Phys. Rev. Lett.*, 80:5243–5246, Jun 1998.

[14] H. Benisty, A. Degiron, A. Lupu, A. De Lustrac, S. Chénais, S. Forget, M. Besbes, G. Barbillon, A. Bruyant, S. Blaize, et al. Implementation of pt symmetric devices using plasmonics: principle and applications. *Optics Express*, 19(19):18004–18019, 2011.

[15] D. Benney and G. J. Roskes. Wave instabilities. *Studies in Applied Mathematics*, 48(4):377–385, 1969.

[16] J. L. Bohn, R. M. Wilson, and S. Ronen. How does a dipolar Bose-Einstein condensate collapse? *Laser Physics*, 19(4):547–549, 2009.

[17] E. Caliceti and S. Graffi. Reality and non-reality of the spectrum of pt-symmetric operators: Operator-theoretic criteria. *Pramana–J. Phys*, 73(2), 2009.

[18] H. Cartarius and G. Wunner. Model of a pt-symmetric Bose-Einstein condensate in a δ-function double-well potential. *Physical Review A*, 86(1):013612, 2012.

[19] J. M. Cerveró and A. Rodríguez. The band spectrum of periodic potentials with pt-symmetry. *Journal of Physics A: Mathematical and General*, 37(43):10167, 2004.

[20] L. Chang, X. Jiang, S. Hua, C. Yang, J. Wen, L. Jiang, G. Li, G. Wang, and M. Xiao. Parity-time symmetry and variable optical isolation in active-passive-coupled microresonators. *Nature photonics*, 8(7):524–529, 2014.

[21] R. Y. Chiao, E. Garmire, and C. H. Townes. Self-trapping of optical beams. *Phys. Rev. Lett.*, 14:1056–1056, Jun 1965.

[22] N. Chtchelkatchev, A. Golubov, T. Baturina, and V. Vinokur. Stimulation of the fluctuation superconductivity by p t symmetry. *Physical Review Letters*, 109(15):150405, 2012.

[23] J. Cole, K. Makris, Z. Musslimani, D. Christodoulides, and S. Rotter. Twofold pt symmetry in doubly exponential optical lattices. *Physical Review A*, 93(1):013803, 2016.

[24] J. T. Cole and Z. H. Musslimani. Band gaps and lattice solitons for the higher-order nonlinear Schrödinger equation with a periodic potential. *Physical Review A*, 90(1):013815, 2014.

[25] J. T. Cole and Z. H. Musslimani. Spectral transverse instabilities and soliton dynamics in the higher-order multidimensional nonlinear Schrödinger equation. *Physica D: Nonlinear Phenomena*, 313:26–36, 2015.

[26] L.-C. Crasovan, J. P. Torres, D. Mihalache, and L. Torner. Arresting wave collapse by wave self-rectification. *Physical review letters*, 91(6):063904, 2003.

[27] A. Davey. On three-dimensional packets of surface waves. *Proc. R. Soc. Lond. A*, 338(1613):101–110, 1974.

[28] E. A. Donley, N. R. Claussen, S. L. Cornish, J. L. Roberts, E. A. Cornell, and C. E. Wieman. Dynamics of collapsing and exploding Bose–Einstein condensates. *Nature*, 412(6844):295, 2001.

[29] M. S. P. Eastham. *The Spectral Theory of Periodic Differential Equations*. Scottish Academic Press [distributed by Chatto & Windus, London, 1973.

[30] C. Eberlein, S. Giovanazzi, and D. H. J. O'Dell. Exact solution of the Thomas-Fermi equation for a trapped Bose-Einstein condensate with dipole-dipole interactions. *Physical Review A*, 71(3):033618, 2005.

[31] J. Eggers and M. A. Fontelos. The role of self-similarity in singularities of partial differential equations. *Nonlinearity*, 22(1):R1, 2008.

[32] C. Eigen, A. L. Gaunt, A. Suleymanzade, N. Navon, Z. Hadzibabic, and R. P. Smith. Observation of weak collapse in a Bose-Einstein condensate. *Physical Review X*, 6(4):041058, 2016.

[33] A. L. Fetter and A. A. Svidzinsky. Vortices in a trapped dilute Bose-Einstein condensate. *Journal of Physics: Condensed Matter*, 13(12):R135, 2001.

[34] G. Fibich. *The Nonlinear Schrödinger Equation: Singular Solutions and Optical Collapse*, volume 192. 2015.

[35] G. Fibich, N. Gavish, and X.-P. Wang. New singular solutions of the nonlinear Schrödinger equation. *Physica D: Nonlinear Phenomena*, 211(3-4):193–220, 2005.

[36] T. D. Grow, A. A. Ishaaya, L. T. Vuong, A. L. Gaeta, N. Gavish, and G. Fibich. Collapse dynamics of super-Gaussian beams. *Opt. Express*, 14(12):5468–5475, Jun 2006.

[37] B. Ilan, Y. Sivan, and G. Fibich. A quantitative approach to soliton instability. *Opt. Lett.*, 36(3):397–399, Feb 2011.

[38] W. Jones and N. H. March. *Theoretical Solid State Physics: Perfect Lattices in Equilibrium*, volume 1. Courier Corporation, 1973.

[39] P. L. Kelley. Self-focusing of optical beams. *Phys. Rev. Lett.*, 15:1005–1008, Dec 1965.

[40] P. G. Kevrekidis, D. J. Frantzeskakis, and R. Carretero-González. *Emergent Nonlinear Phenomena in Bose-Einstein Condensates: Theory and Experiment*, volume 45. Springer Science & Business Media, 2007.

[41] C. Kittel and D. F. Holcomb. *Introduction to Solid State Physics*, volume 35. American Association of Physics Teachers, 1967.

[42] P. T. Krein, J. Bentsman, R. M. Bass, and B. L. Lesieutre. On the use of averaging for the analysis of power electronic systems. *IEEE Transactions on Power Electronics*, 5(2):182–190, 1990.

[43] P. A. Kuchment. *Floquet Theory for Partial Differential Equations*, volume 60. Birkhäuser, 2012.

[44] T. Lahaye, C. Menotti, L. Santos, M. Lewenstein, and T. Pfau. The physics of dipolar bosonic quantum gases. *Reports on Progress in Physics*, 72(12):126401, 2009.

[45] T. Lahaye, J. Metz, B. Froehlich, T. Koch, M. Meister, A. Griesmaier, T. Pfau, H. Saito, Y. Kawaguchi, and M. Ueda. d-wave collapse and explosion of a dipolar Bose-Einstein condensate. *Physical review letters*, 101(8):080401, 2008.

[46] E. H. Lieb, R. Seiringer, and J. Yngvason. Bosons in a trap: A rigorous derivation of the Gross-Pitaevskii energy functional. In *The Stability of Matter: From Atoms to Stars*, pages 685–697. Springer, 2001.

[47] P. M. Lushnikov. Collapse of Bose-Einstein condensates with dipole-dipole interactions. *Physical Review A*, 66(5):051601, 2002.

[48] P. M. Lushnikov. Collapse and stable self-trapping for Bose-Einstein condensates with 1/r b-type attractive interatomic interaction potential. *Physical Review A*, 82(2):023615, 2010.

[49] K. Makris, R. El-Ganainy, D. Christodoulides, and Z. H. Musslimani. Pt-symmetric periodic optical potentials. *International Journal of Theoretical Physics*, 50(4):1019–1041, 2011.

[50] K. G. Makris, R. El-Ganainy, D. N. Christodoulides, and Z. H. Musslimani. Pt-symmetric optical lattices. *Physical Review A*, 81(6):063807, 2010.

[51] F. Merle, P. Raphaël, and J. Szeftel. Stable self-similar blow-up dynamics for slightly l 2 super-critical NLS equations. *Geometric and Functional Analysis*, 20(4):1028–1071, 2010.

[52] J. Metz, T. Lahaye, B. Fröhlich, A. Griesmaier, T. Pfau, H. Saito, Y. Kawaguchi, and M. Ueda. Coherent collapses of dipolar Bose–Einstein condensates for different trap geometries. *New Journal of Physics*, 11(5):055032, 2009.

[53] K. D. Moll, A. L. Gaeta, and G. Fibich. Self-similar optical wave collapse: observation of the Townes profile. *Physical Review Letters*, 90(20):203902, 2003.

[54] Z. H. Musslimani, K. G. Makris, R. El-Ganainy, and D. N. Christodoulides. Analytical solutions to a class of nonlinear Schrodinger equations with PT-like potentials. *Journal of Physics A – Mathematical and Theoretical*, 41(24), 2008.

[55] S. Nixon and J. Yang. Nonlinear wave dynamics near phase transition in pt-symmetric localized potentials. *Physica D: Nonlinear Phenomena*, 331:48–57, 2016.

[56] D. H. J. O'Dell, S. Giovanazzi, and C. Eberlein. Exact hydrodynamics of a trapped dipolar Bose-Einstein condensate. *Physical Review Letters*, 92(25):250401, 2004.

[57] P. Pedri and L. Santos. Two-dimensional bright solitons in dipolar Bose-Einstein condensates. *Phys. Rev. Lett.*, 95:200404, Nov 2005.

[58] C. J. Pethick and H. Smith. *Bose-Einstein Condensation in Dilute Gases*. Cambridge University Press, 2 edition, 2008.

[59] M. C. Rechtsman, J. M. Zeuner, Y. Plotnik, Y. Lumer, D. Podolsky, F. Dreisow, S. Nolte, M. Segev, and A. Szameit. Photonic Floquet topological insulators. *Nature*, 496(7444):196–200, 2013.

[60] M. Reed and B. Simon. *IV: Analysis of Operators*, volume 4. Elsevier, 1978.

[61] P. Robinson. Nonlinear wave collapse and strong turbulence. *Rev. Mod. Phys.*, 69:507, 1997.

[62] J. Rubinstein, P. Sternberg, and Q. Ma. Bifurcation diagram and pattern formation of phase slip centers in superconducting wires driven with electric currents. *Physical Review Letters*, 99(16):167003, 2007.

[63] J. Rubinstein, P. Sternberg, and K. Zumbrun. The resistive state in a superconducting wire: bifurcation from the normal state. *Archive for Rational Mechanics and Analysis*, 195(1):117–158, 2010.

[64] K. C. Shin. On the shape of spectra for non-self-adjoint periodic Schrödinger operators. *Journal of Physics A: Mathematical and General*, 37(34):8287, 2004.

[65] A. Shkalikov. Spectral portraits of the Orr-Sommerfeld operator with large Reynolds numbers. *Journal of Mathematical Sciences*, 124(6):5417–5441, 2004.

[66] Y. Sivan, G. Fibich, B. Ilan, and M. I. Weinstein. Qualitative and quantitative analysis of stability and instability dynamics of positive lattice solitons. *Physical Review E - Statistical, Nonlinear, and Soft Matter Physics*, 78(4), 2008.

[67] R. H. Stolen. The early years of fiber nonlinear optics. *Journal of Lightwave Technology*, 26(9):1021–1031, May 2008.

[68] C. Sulem and P. L. Sulem. The Nonlinear Schrödinger Equation: Self-Focusing and Wave Collapse. *Applied Mathematical Sciences*, 139(139):xvi, 350 p., 1999.

[69] T. Taha and M. Ablowitz. Analytical and numerical aspects of certain nonlinear evolution equations. II. Numerical, nonlinear Schrödinger equation. *Journal of Computational Physics*, 55(2):203–230, 1984.

[70] C. Ticknor, R. M. Wilson, and J. L. Bohn. Anisotropic superfluidity in a dipolar Bose gas. *Physical Review Letters*, 106(6):065301, 2011.

[71] I. Tikhonenkov, B. A. Malomed, and A. Vardi. Anisotropic solitons in dipolar Bose-Einstein condensates. *Physical Review Letters*, 100(9):090406, 2008.

[72] N. Vakhitov and A. A. Kolokolov. Stationary solutions of the wave equation in a medium with nonlinearity saturation. *Radiophysics and Quantum Electronics*, 16(7):783–789, 1973.

[73] L. T. Vuong, T. D. Grow, A. Ishaaya, A. L. Gaeta, G. W. 't Hooft, E. R. Eliel, and G. Fibich. Collapse of optical vortices. *Physical Review Letters*, 96(13):133901, 2006.

[74] R. M. Wilson, S. Ronen, and J. L. Bohn. Angular collapse of dipolar Bose-Einstein condensates. *Physical Review A*, 80(2):023614, 2009.

[75] J. Yang and T. I. Lakoba. Accelerated imaginary-time evolution methods for the computation of solitary waves. *Studies in Applied Mathematics*, 120(3):265–292, 2008.

[76] S. Yi and L. You. Trapped condensates of atoms with dipole interactions. *Physical Review A*, 63(5):053607, 2001.

[77] B. W. Zeff, B. Kleber, J. Fineberg, and D. P. Lathrop. Singularity dynamics in curvature collapse and jet eruption on a fluid surface. *Nature*, 403(6768):401, 2000.